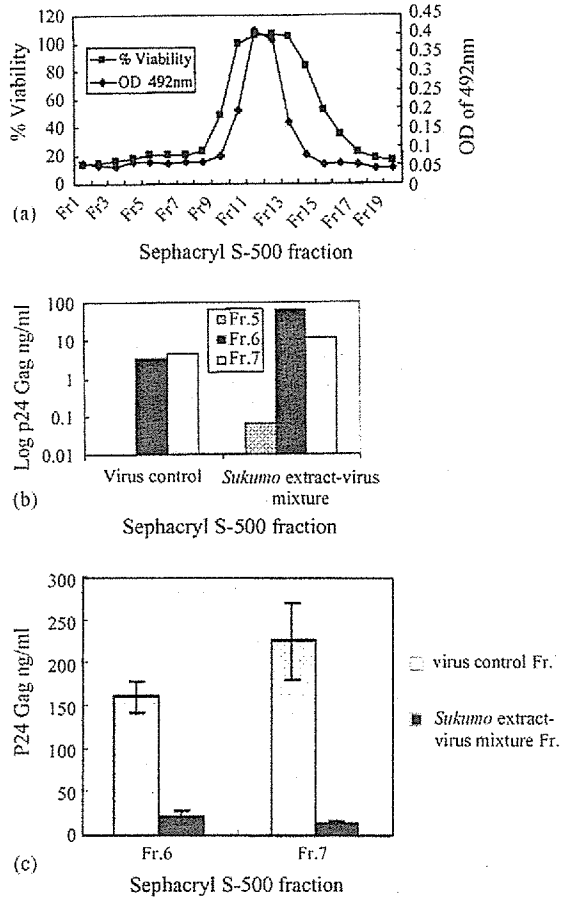

Fig. 4. Specific binding of *Sukumo* extract to HIV-1 virions, resulting in viral entry blockade and inhibition of HIV-1 replication in MT-4 cells. Experiments were carried out with a Sephacryl S-500 column in which three samples of *Sukumo* extract control, virus control (HIV NL4-3) and *Sukumo* extract–virus mixture were separated with a chromatograph column, respectively. (A) Anti-HIV-1 activity and absorbance of the wavelength of 492 nm from chromatogram fractions of *Sukumo* extract control eluate. Absorbance of *Sukumo* extract control fractions was measured at the wavelength of 492 nm (♦); the activity of each fraction was tested against HIV-1 replication by MTT assay, and then the viability of cells was calculated (■). (B) The quantity of HIV-1 p24 Gag was measured by auto-ELISA p24 Gag assay from chromatogram fractions 5–7 of virus control eluate and *Sukumo* extract–virus mixture eluate. (C) Infectivity of HIV-1 NL4-3 from chromatogram fractions of the virus control and *Sukumo* extract–virus mixture. The eluted fractions 6 and 7 were selected and infected into MT-4 cells for 2 h at 37 °C. After washing, the cells were incubated for 4 days and p24 Gag of culture supernatant was measured by auto-ELISA.

(Fig. 4A). On the other hand, HIV-1 was eluted in fractions 6 and 7 as shown by p24 assay (Fig. 4B left). When an excess amount of *Sukumo* extract was mixed with HIV-1 and separated with Sephacryl, the viral peak was detected in fractions 6 and 7 once again (Fig. 4B right), while anti-HIV activity was still observed in fraction 10–14 (data not shown). To see whether these fractions contained an infective capacity of HIV-1, the amount of p24 Gag was assessed in the supernatant of MT-4 cells after infection. We used the same volume (150 μl) of eluted fractions 6 and 7 from viral control, which contained 0.53 and 0.69 ng of p24 antigen, or those from the *Sukumo* extract–virus mixture which contained 10.24 and 1.78 ng of p24 antigen to infect 4×10^5 MT-4 cells, respectively. As shown in Fig. 4C, fractions 6 and 7 obtained from the viral control exhibited high HIV-1 activity (161.35 and 226.32 ng/ml in p24 level) 4 days after infection while fractions 6 and 7 from the *Sukumo* extract–virus mixture had p24 levels as low as 21.6 and 13.76 ng/ml, respectively. These results strongly suggests that the *Sukumo* extract specifically bound to viral particles and was efficiently trapped by viral particles so that viral infectivity was significantly abrogated due to the blockage of entry into the cells.

3.5. Effect of Sukumo extract on VSV-G pseudotyped HIV-1 replication

Although all the data provided evidence that HIV-1 entry could be a primary anti-viral target of *Sukumo* extract, there still remained the possibility that *Sukumo* extract exerts its effect on a late step of viral replication. To address this, a time course assay was performed using a single cycle infection with VSV-G pseudotyped HIV-1 and 293T cells. P24 Gag in the supernatant was measured 3 days post-infection. The result showed that a dose-dependent anti-viral activity of *Sukumo* extract was observed when it was added at the time B (entry) step. In contrast, the inhibition was not seen when *Sukumo* extract was added at the time A (pre-treatment) or time C step (post-entry) at any concentrations studied (range 0.16–100 μg/ml) (Fig. 5). A similar result was also observed when Hos/CD4-CCR5 cells were used (data not shown). These results suggest that *Sukumo* extract does affect an early step, not a post-entry step, of the viral life cycle.

Based on these studies, we conclude that there is persuasive evidene that *Sukumo* extract is a binding inhibitor that interferes with virion/cells interactions and that this inhibition is likely mediated through binding to the HIV-1 viral envelope.

3.6. Physico-chemical characterization of anti-viral factors in Sukumo extract

The anti-viral factor was extracted from *Sukumo* using organic solvent and water. Inhibitory activity was found in the aqueous extract. Crude *Sukumo* extract was fractionated by DEAE-Sephacel column chromatography. The main fractions which had anti-viral activity was eluted from the column by 1.0–2.0 M NaCl (Fig. 6A). The *Sukumo* extract was also separated by using SDS-PAGE and anti-HIV-1 activity was detected in fractions 3–7 of the SDS-gel extracts corresponding to a molecular weight of 10,000–50,000 (Fig. 6B). Gas chromatography analysis of the acid hydrolysates of the *Sukumo* extract revealed the carbohydrate contents of Ara:Xyl:Man:Gal:Glc were 5.1:1:2.1:3.3:2.6 (Table 1) and SDS-PAGE/PAS staining yielded a bright red band (Zacharius et al., 1969) (data not shown). Elemental analysis revealed that the sulfer content is 1.14% in the

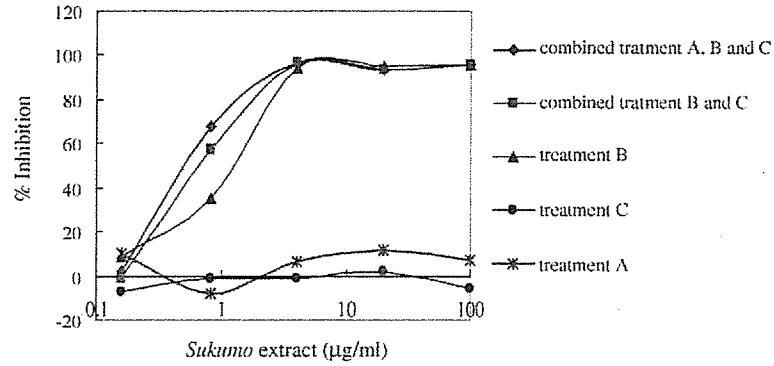

Fig. 5. Effect of *Sukumo* extract on VSV-G pseudotyped HIV-1 replication. 293T cells were infected with the HIV-1 NL-E strain lacking env and nef with VSV-G envelope of pesudotyped virus. 0.16–100 μg/ml *Sukumo* extract was used and anti-HIV-1 activity was determined 3 days later by measuring p24 Gag. Treatment A (a pre-entry step): the cells were incubated with *Sukumo* extract for 2 h at 37 °C and washed before exposure to virus, and then the cells were infected and incubated in the absence of *Sukumo* extract. Treatment B (an entry step): the cells were exposed to virus in the presence of *Sukumo* extract for 2 h, then both *Sukumo* extract and unabsorbed viruses were removed by washing. The cells were further incubated in the absence of *Sukumo* extract. Treatment C (a post-entry step): the cells were infected with virus for 2 h, unabsorbed virus were removed and further incubated in presence of *Sukumo* extract.

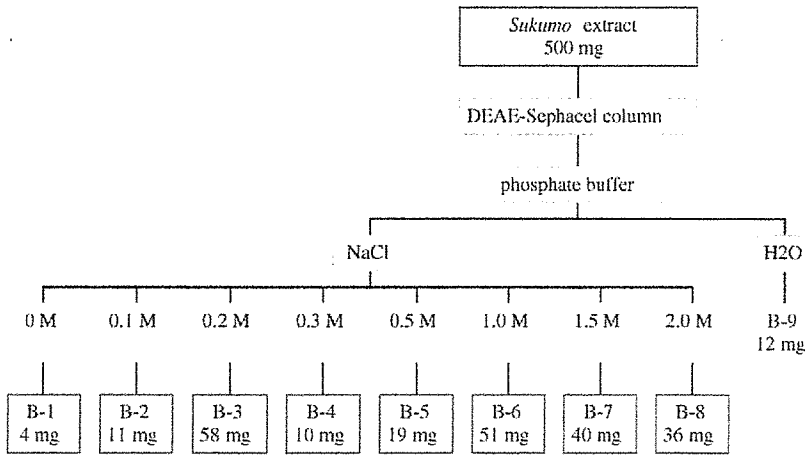

(A)

Fr.	EC_{50} μg/ml
B-1	>100
B-2	>100
B-3	>100
B-4	>100
B-5	>100
B-6	0.7405
B-7	0.6155
B-8	0.8818
B-9	9.7729

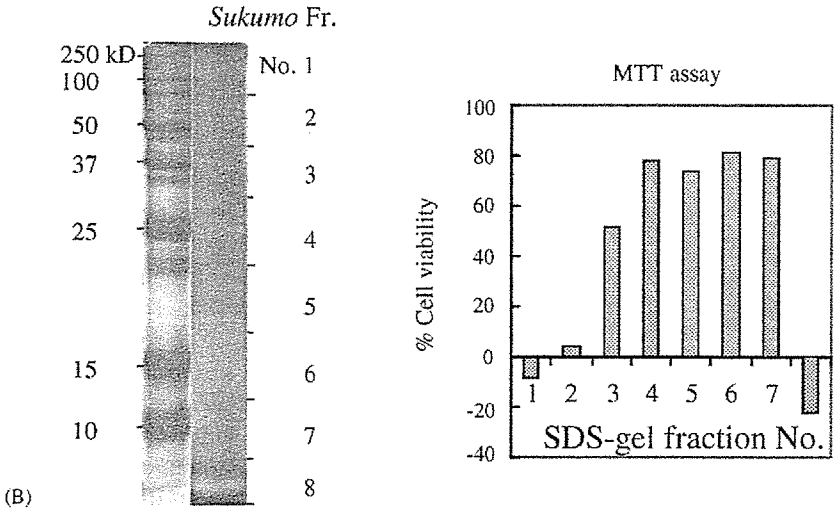

(B)

Fig. 6. Physico-chemical characterization of *Sukumo* extract. (A) *Sukumo* extract was analyzed with a DEAE-Sephacel column. The anti-HIV-1 activity of each eluting fraction was tested by MTT assay. The antiviral factor was eluted in 1.0–2.0 M NaCl. (B) *Sukumo* extract was analyzed by SDS-PAGE. 0.4 mg of *Sukumo* extract was separated with 15% SDS-PAGE. The gel was stained with silver reagent for protein analysis. The anti-HIV-1 activities of extracts from SDS-gel fractions were tested by MTT assay.

Table 1
Compound properties of *Sukumo* extract

Amino acid (%)	Carbohydrate[a]	Molar ratio	Element	Percentage (%)
0.002	Arabinose	5.1	H	4.14
	Xylose	1	C	37.16
	Mannose	2.1	N	6.66
	Galactose	3.3	S	1.14
	Glucose	2.6		
	Rhamnose	Trace		

[a] The *Sukumo* extract was hydrolyzed with 1 M H_2SO_4 at 100 °C for 6 h, and then the solution was applied on Supelco SP-2380 column and was analyzed with Shimadzu gas cells chromatograph GC-14B.

Sukumo extract (Table 1). The anti-viral factor in *Sukumo* extract was stable under a wide range of pH conditions. As shown in Table 2, the anti-viral activity of *Sukumo* extract was not reduced after treatment with 6N H_2SO_4, 1N HCl or $NaIO_4$, but the value of EC_{50} (1.095 μg/ml) was somewhat decreased when it was treated with 1N NaOH. The activity was also not lost after being heated at 121 °C for 20 min and was not inactivated by protease (trypsin, proteinase K and pronase) digestion. Finally, we addressed whether the anti-HIV-1 activities of *Sukumo* extract, heparin and dextran sulfate were abrogated after they were treated with acid. When *Sukumo* extract was boiled at 100 °C in 6N H_2SO_4 and 1N HCl for 6 h the 50% effective concentration (EC_{50}) against HIV-1 was essentially unaffected. In sharp contrast, when heparin was boiled at 100 °C in 6N H_2SO_4 for 6 h or dextran sulfate in 1N HCl for 2 h, the 50% effective concentrations against HIV-1 were >940 and >1000 μg/ml by MTT assay, while those of the untreated samples were 8.2095 and 0.7707 μg/ml, respectively (Table 2).

Table 2
Effect of various physico-chemical treatments on anti-HIV-1 (III_B) activity of *Sukumo* extract in MT-4

Treated with	Compound[a] (EC_{50} μg/ml)		
	Sukumo extract	Heparin	Dextran sulfate (MW 500,000)
Untreated	0.5891	8.2095	0.7016
121 °C 20 min	0.5166	ND[f]	ND[f]
Trypsin[b]	0.6686	ND	ND
Proteinase K[b]	0.5727	ND	ND
Pronase[b]	0.4736	ND	ND
NaOH[c]	1.0954	ND	ND
$NaIO_4$[d]	0.5832	ND	ND
H_2SO_4 treated[e]	0.4155	>940	ND
HCl treated[e]	0.7707	ND	>1000

[a] The 50% effective concentration was determined by MTT assay using HIV-1 (III_B) strain and MT-4 cells.

[b] The *Sukumo* extract was digested by trypsin (Sigma) (0.5–1 mg/ml at a final concentration), proteinase K (100 ng/ml) and pronase (Fluka) (0.2 mg/ml) at 37 °C for 30 h. The digestions were terminated by boiling the solution for 20 min at 100 °C.

[c] The *Sukumo* extract was boiled at 100 °C for 6 h in the presence of 1N NaOH.

[d] The *Sukumo* extract was incubated at 4 °C for 40 h in the presence of 100 mM $NaIO_4$. After treatment, the *Sukumo* extract was precipitated with 2 volumes of ethanol and resuspended in 1 volume of H_2O.

[e] Each compound was boiled at 100 °C for 6 h in the presence of 6N H_2SO_4 or for 2 h in the presence of 1N HCl. After treatment, pH was adjusted to 7.5.

[f] ND: not determined.

4. Discussion

Sukumo extract potently and selectively inhibited HIV-1 replication in vitro. The compound was also evaluated for activity against various virus species with or without an envelope including vesicular stomatitis virus G protein enveloped HIV-1 pseudotyped type virus. Whereas *Sukumo* extract was active against herpes simplex virus, it was devoid of any activity against influenza A virus, SARS virus and a non-enveloped poliovirus.

Based on the current knowledge of HIV, several stages of the viral life cycle are potentially vulnerable to inhibitors. These can be divided into the entry steps and post-entry steps. In this study, we have demonstrated by several different techniques that *Sukumo* extract inhibits the HIV-1 infectious process at the cell entry step. The data presented in Fig. 3 indicate that *Sukumo* extract is able to block viral binding to target cells and inhibits virus-induced cell–cell fusion. Furthermore, a time-course experiment showed that the full protective activity of *Sukumo* extract was achieved when the compound was present during the 2-h virus adsorption period, but none of the effect was seen when the compound was incubated with the cells prior to viral infection. Also, the extract did not suppress the viral replication after the virus had entered the cells. Thus, *Sukumo* extract interferes with an early event of the virus replication cycle, most presumably the viral adsorption step.

Two classes of cell surface molecules, CD4 and chemokine receptors, as well as CCR5 or CXCR4, are often viewed as HIV coreceptors which mediate HIV-1 entry. We found that the down-modulation of HIV-1 receptor CD4 or co-receptor CCR5 in target cells was induced by the *Sukumo* extract. However, the inhibitory activity was rather weak. In addition, this activity of *Sukumo* extract was lost if the cells were washed prior to addition of antibody, indicating that the compounds can only weakly associate with the cell surface. Therefore, the results cannot perfectly explain why the *Sukumo* extract is able to block virus entry of HIV so efficiently, especially the R5 HIV-1 virus.

The effect of *Sukumo* extract on the viral binding process was assessed directly, using a chromatography method (Fig. 4). The results show that *Sukumo* extract was bound to HIV-1 and was separated along with the larger virus particle fraction from a gel filtration column. From this study we hypothesized that *Sukumo* extract exerts its anti-HIV activity by binding to the viral envelope glycoprotein. This results in prevention of virus attachment to the cell surface receptor or co-receptor, whereby interference with early adsorption and entry into the HIV replicative cycle. These findings are

consistent with the hypothesis that *Sukumo* extract interferes with virions rather than cell function. It might also explain why *Sukumo* extract is less toxic to target cells in vitro.

The biochemical features of water extract of *Sukumo* prepared from *Polygonum tinctorium* that selectively inhibited the replication of HIV-1 were studied. The anti-viral activity was extracted from *Sukumo* in a variety of ways, using water and organic solvents (hexane, chloroform, acetone and ethanol). Inhibitory activity was found in the aqueous extracts, whereas the extracts by organic solvents did not show any anti-HIV activity. Indigo, a staining ingredient and tryptanthrin, a low molecular weight component from *Polygonum tinctorium*, also did not exihibit any anti-HIV activity (data not shown).

The main fraction of anti-HIV activity was eluted from the DEAE-Sephacel column, a negative ion-exchange column at higher molar (1.0–2.0) NaCl. This result indicate that the active factor(s) is highly anionic. It was also confirmed that the anti-HIV compound(s) consist of phenolic substructure by $FeCl_3$–$K_3Fe(CN)_6$ staining (Barton et al., 1952) (data not shown) and a polysaccharide containing sulfur atom by sugar analysis and elemental analysis, respectively (Table 1). The factor was estimated to be a high molecular weight compound of 10,000–50,000 by Sephadex G-75 gel-filtration analysis (data not shown) and an SDS-gel of *Sukumo* extract (Fig. 6B). No protein was detected in the water extract of *Sukumo* with SDS-PAGE/silver staining. The data confirm our observation that the inhibitory activity of *Sukumo* extract was not inactivated by protease digestion or heating at 121 °C for 20 min. Furthermore, boiling of the *Sukumo* extract in the presence of 1N HCl, 6N H_2SO_4 and 1N NaOH for 6 h did not result in any loss of this activity. Similarly, it was not inactivated by $NaIO_4$ treatment (Nakashima et al., 1987b), which breaks down carbohydrates (Table 2). This suggests that the sugar backbone is not essential for the anti-HIV activity of the *Sukumo* extract. The pharmaceutical value of the *Sukumo* extract is likely to be further enhanced by its stability over a wide range of pH values, as shown by the heating at 121 °C 20 min and treatment with acid and alkaline conditions. Since the anti-HIV-1 activity of *Sukumo* was higher than that of fresh leaves (data not shown), the possibility that the active substances were derived from bacteria could not be excluded.

We compared difference between representative sulfated polysaccharides and *Sukumo* extract for their susceptibility to acid treatment. The anti-HIV-1 effect was clearly abrogated by this treatment in the case of dextran sulfate and heparin, but not *Sukumo* extract (Table 2). The anti-HIV-1 activity of heparin was completely destroyed by 6N H_2SO_4 treatment as in the case of 1N HCl treatment of dextran sulfate. Unlike epigallocatechin gallate, a polyphenolic substance from green tea (Suzutani et al., 2003; Yamaguchi et al., 2002), *Sukumo* extract did not exert any anti-HIV-1 activity on the post-virus entry process. Further work on the characterization of the *Sukumo* extract and its potency as an anti-viral candidate drug is in progress.

Acknowledgements

The authors thank Dr. Fumio Shaku for performing the infection of HSV-1 experiments and gift of wild-type herpes simplex virus 1 and Vero cells. This work was supported by grants from the Ministry of Education, Science, and Culture and the Ministry of Health, Labor, and Welfare of Japan. The manuscript was reviewed prior to submission by Pacific Edit.

References

Baba, M., Pauwels, R., Balzarini, J., Arnout, J., Desmyter, J., De Clercq, E., 1988. Mechanism of inhibitory effect of dextran sulfate and heparin on replication of human immunodeficiency virus in vitro. Proc. Natl. Acad. Sci. U.S.A. 85, 6132–6136.

Bartolini, B., Di Caro, A., Cavallaro, R.A., Liverani, L., Mascellani, G., La Rosa, G., Marianelli, C., Muscillo, M., Benedetto, A., Cellai, L., 2003. Susceptibility to highly sulphated glycosaminoglycans of human immunodeficiency virus type 1 replication in peripheral blood lymphocytes and monocyte-derived macrophages cell cultures. Antiviral Res. 58, 139–147.

Barton, G.M., Evans, R.S., Gardner, J.A.F., 1952. Paper chromatography of phenolic substances. Nature 170, 249–250.

Honda, G., Tabata, M., 1979. Isolation of antifungal principle tryptathrin, from Strobilanthes cusia O. Kuntze. Planta Med. 36, 85–86.

Ichiyama, K., Yokoyama-Kumakura, S., Tanaka, Y., Tanaka, R., Hirose, K., Bannai, K., Edamatsu, T., Yanaka, M., Niitani, Y., Miyano-Kurosaki, N., Takaku, H., Koyanagi, Y., Yamamoto, N., 2003. A duodenally absorbable CXC chemokine receptor 4 antagonist, KRH-1636, exhibits a potent and selective anti-HIV-1 activity. Proc. Natl. Acad. Sci. U.S.A. 100, 4185–4190.

Kataoka, M., Hirata, K., Kunikata, T., Ushio, S., Iwaki, K., Ohashi, K., Ikeda, M., Kurimoto, M., 2001. Antibacterial action of tryptanthrin and kaempferol, isolated from the indigo plant (*Polygonum tinctorium* Lour.), against Helicobacter pylori-infected Mongolian gerbils. J. Gastroenterol. 36, 5–9.

Kim, H.M., Hong, D.R., Lee, E.H., 1998. Inhibition of mast cell-dependent anaphylactic reactions by the pigment of *Polygonum tinctorium* (Chung-Dae) in rats. Gen. Pharmacol. 31, 361–365.

Koya-Miyata, S., Kimoto, T., Micallef, M.J., Hino, K., Taniguchi, M., Ushio, S., Iwaki, K., Ikeda, M., Kurimoto, M., 2001. Prevention of azoxymethane-induced intestinal tumors by a crude ethyl acetate-extract and tryptanthrin extracted from *Polygonum tinctorium* Lour. Anticancer Res. 21, 3295–3300.

Lin, Y.L., Mettling, C., Portales, P., Reynes, J., Clot, J., Corbeau, P., 2002. Cell surface CCR5 density determines the postentry efficiency of R5 HIV-1 infection. Proc. Natl. Acad. Sci. U.S.A. 99, 15590–15595.

Miyake, M., Arai, N., Ushio, S., Iwaki, K., Ikeda, M., Kurimoto, M., 2003. Promoting effect of kaempferol on the differentiation and mineralization of murine pre-osteoblastic cell line MC3T3-E1. Biosci. Biotechnol. Biochem. 67, 1199–1205.

Moore, J.P., Stevenson, M., 2000. New targets for inhibitors of HIV-1 replication. Nat. Rev. Mol. Cell Biol. 1, 40–49.

Moulard, M., Lortat-Jacob, H., Mondor, I., Roca, G., Wyatt, R., Sodroski, J., Zhao, L., Olson, W., Kwong, P.D., Sattentau, Q.J., 2000. Selective interactions of polyanions with basic surfaces on human immunodeficiency virus type 1 gp120. J. Virol. 74, 1948–1960.

Nakashima, H., Kido, Y., Kobayashi, N., Motoki, Y., Neushul, M., Yamamoto, N., 1987a. Purification and characterization of an avian myeloblastosis and human immunodeficiency virus reverse transcriptase inhibitor, sulfated polysaccharides extracted from sea algae. Antimicrob. Agents Chemother. 31, 1524–1528.

Nakashima, H., Kido, Y., Kobayashi, N., Motoki, Y., Neushul, M., Yamamoto, N., 1987b. Antiretroviral activity in a marine red alga: reverse transcriptase inhibition by an aqueous extract of *Schizymenia pacifica*. J. Cancer Res. Clin. Oncol. 113, 413–416.

Nakashima, H., Yoshida, O., Baba, M., De Clercq, E., Yamamoto, N., 1989. Anti-HIV activity of dextran sulphate as determined under different experimental conditions. Antiviral Res. 11, 233–246.

Nakashima, H., Murakami, T., Yamamoto, N., Sakagami, H., Tanuma, S., Hatano, T., Yoshida, T., Okuda, T., 1992. Inhibition of human immunodeficiency viral replication by tannins and related compounds. Antiviral Res. 18, 91–103.

Santhosh, K.C., Paul, G.C., De Clercq, E., Pannecouque, C., Witvrouw, M., Loftus, T.L., Turpin, J.A., Buckheit Jr., R.W., Cushman, M., 2001. Correlation of anti-HIV activity with anion spacing in a series of cosalane analogues with extended polycarboxylate pharmacophores. J. Med. Chem. 44, 703–714.

Suzutani, T., Ogasawara, M., Yoshida, I., Azuma, M., Knox, Y.M., 2003. Anti-herpesvirus activity of an extract of *Ribes nigrum* L. Phytother. Res. 17, 609–613.

Witvrouw, M., De Clercq, E., 1997. Sulfated polysaccharides extracted from sea algae as potential antiviral drugs. Gen. Pharmacol. 29, 497–511.

Yamaguchi, K., Honda, M., Ikigai, H., Hara, Y., Shimamura, T., 2002. Inhibitory effects of (−)-epigallocatechin gallate on the life cycle of human immunodeficiency virus type 1 (HIV-1). Antiviral Res. 53, 19–34.

Ylisastigui, L., Bakri, Y., Amzazi, S., Gluckman, J.C., Benjouad, A., 2000. Soluble glycosaminoglycans do not potentiate RANTES antiviral activity on the infection of primary macrophages by human immunodeficiency virus type 1. Virology 278, 412–422.

Zacharius, R.M., Zell, T.E., Morrison, J.H., Woodlock, J.J., 1969. Glycoprotein staining following electrophoresis on acrylamide gels. Anal Biochem. 30, 148–152.

Small peptide inhibitors of the CXCR4 chemokine receptor (CD184) antagonize the activation, migration, and antiapoptotic responses of CXCL12 in chronic lymphocytic leukemia B cells

Meike Burger, Tanja Hartmann, Myriam Krome, Justyna Rawluk, Hirokazu Tamamura, Nobutaka Fujii, Thomas J. Kipps, and Jan A. Burger

Growth and survival of chronic lymphocytic leukemia (CLL) B cells are favored by interactions between CLL and nontumoral accessory cells. CLL cells express CXCR4 chemokine receptors that direct leukemia cell chemotaxis. Marrow stromal cells or nurselike cells constitutively secrete CXCL12, the ligand for CXCR4, thereby attracting and rescuing CLL B cells from apoptosis in a contact-dependent fashion. Therefore, the CXCR4-CXCL12 axis represents a potential therapeutic target in CLL. We evaluated the most active CXCR4-specific antagonists (T140, TC14012, TN14003) for their capacity to inhibit CXCL12 responses in CLL cells. T140, or its analogs, inhibited actin polymerization, chemotaxis, and migration of CLL cells beneath stromal cells. CXCL12-induced phosphorylation of p44/42 mitogen-activated protein kinase (MAPK) and signal transducer and activator of transcription 3 (STAT3) was abolished by CXCR4 antagonists. TC14012 and TN14003 antagonized the antiapoptotic effect of synthetic CXCL12 and stromal cell–mediated protection of CLL cells from spontaneous apoptosis. Furthermore, we found that stromal cells protected CLL cells from chemotherapy-induced apoptosis. Treatment with CXCR4 antagonists resensitized CLL cells cultured with stromal cells to fludarabine-induced apoptosis. These findings demonstrate that CXCR4 blocking agents effectively antagonize CXCL12-induced migratory and signaling responses and stromal protection of CLL cells from spontaneous or fludarabine-induced apoptosis. As such, small molecular CXCR4 antagonists may have activity in the treatment of patients with this disease. (Blood. 2005;106:1824-1830)

Introduction

B-cell chronic lymphocytic leukemia (CLL) is characterized by the accumulation of a monoclonal population of $CD5^+$ neoplastic B cells in secondary lymphoid organs, marrow, and blood. Because most of the circulating leukemia cells are arrested in the G_0/G_1 phase of the cell cycle, the primary defect may be one of resistance to programmed cell death rather than accelerated cell division.[1,2] However, CLL cells can rapidly undergo spontaneous apoptosis under culture conditions that support the growth of human B-cell lines. This implies that such ex vivo conditions lack factors necessary for leukemia cell survival or that the resistance to apoptosis is not intrinsic to the leukemia B cell.

The leukemia cell microenvironment in the marrow or in secondary lymphoid tissues may contribute to the noted resistance of CLL cells to apoptosis in vivo.[3,4] Normal B-cell development depends on complex interactions with accessory cells that define the so-called specialized microenvironments. T cells and a variety of different types of adherent cells, generally defined as stromal cells, are the main elements of the microenvironment.[3] In patients with CLL, the marrow invariably is infiltrated with CLL B cells, and the pattern and extent of marrow involvement correlates with clinical stage and prognosis.[5,6] As such, interactions with stromal cells in the marrow microenvironment appear to play a role in disease progression and resistance to therapy.[7-9]

In addition, we found that a small proportion of the mononuclear cells from the blood of patients with CLL can differentiate into large, round, adherent cells that attract CLL cells and protect them from undergoing spontaneous or drug-induced cell death.[10,11] Because these cells share features with thymic nurse cells that nurture developing thymocytes, we designated them nurselike cells (NLCs). Although NLCs differentiate from blood mononuclear cells after several days in vitro, fully differentiated NLCs can be found in the spleen and secondary lymphoid tissue of patients with CLL,[11] where they might play a role in protecting CLL cells from apoptosis in vivo. This model implies that CLL cells depend on specific extrinsic factors from NLCs and other stromal elements for their survival. Conceivably, CLL cells recirculate from the blood through secondary lymphoid tissues and back into the systemic circulation in response to certain chemokines.

One such chemokine is stromal cell–derived factor-1/pre–B cell growth-stimulating factor (SDF-1/PBSF), which recently has been designated CXCL12. CXCL12 is a member of a family of chemotactic cytokines (chemokines) that initially were characterized as growth-stimulating factors for B-cell precursors.[12] CXCR4 is a primary physiologic receptor for CXCL12 and functions as a coreceptor for entry of T-tropic strains of HIV-1. Mutant mice with targeted gene disruption of CXCL12 or CXCR4 have defects in the

From the Division of Hematology/Oncology, Department of Medicine, Freiburg University Hospital, Freiburg, Germany; the Graduate School of Pharmaceutical Sciences, Kyoto University, Kyoto, Japan; and the Division of Hematology/Oncology, Department of Medicine, University of California, San Diego, CA.

Submitted January 4, 2005; accepted May 9, 2005. Prepublished online as *Blood* First Edition Paper, May 19, 2005; DOI 10.1182/blood-2004-12-4918.

Supported by Deutsche José Carreras Leukämiestiftung grant DJCLS R02/08 (J.A.B.), Deutsche Forschungsgemeinschaft (DFG) grant BU/1159/3-1 (M.B.), and Deutsche Krebshilfe grant 10-1688-Bu (J.A.B.).

Reprints: Jan A. Burger, Department of Medicine, Division of Hematology/Oncology, Freiburg University Hospital, Hugstetterstr 55, D-79106 Freiburg, Germany; e-mail: burger@mm11.ukl.uni-freiburg.de.

The publication costs of this article were defrayed in part by page charge payment. Therefore, and solely to indicate this fact, this article is hereby marked "advertisement" in accordance with 18 U.S.C. section 1734.

production of new B cells, implicating an important role for CXCL12 in the regulation of early B-cell development.

We previously demonstrated that stromal cells can attract CLL cells through the production of CXCL12.[13] In addition, NLCs express CXCL12 and can attract CLL cells by elaboration of this chemokine.[10] Because CXCL12 may attract leukemia cells to stromal cells and NLCs in vivo, the inhibition of CXCL12-CXCR4 interactions may disrupt the interactions of leukemia cells with protective microenvironments, possibly rendering the CLL cells or other CXCL12-dependent leukemia cells[14] more susceptible to spontaneous or drug-induced apoptosis. Because of this, we examined whether the CXCR4-specific chemokine receptor antagonist T140, a 14-residue polypeptide downsized from a naturally occurring horseshoe crab self-defense peptide, and its analogs[15] could modulate CXCL12-induced activation and survival of CLL B cells and related signaling cascades. In addition, we examined whether CXCR4 receptor antagonists could inhibit the protective effect of stromal cells or NLCs on leukemia cell survival and drug-induced apoptosis.

Patients, materials, and methods

Cell purification, cell culture, chemokines, antibodies, and flow cytometry

After informed consent, blood samples were collected from patients at Freiburg University Hospital who fulfilled diagnostic and immunophenotypic criteria for common B-cell CLL. The patients had not been previously treated with fludarabine and had not received recombinant growth factors or exogenous cytokines. CLL B cells were isolated by density-gradient centrifugation over Ficoll-Hypaque (Pharmacia, Uppsala, Sweden). Cells were used fresh or viably frozen in fetal calf serum containing 5% dimethyl sulfoxide for storage in liquid nitrogen. The viability of CLL cells after recovery was always greater than 85%. All CLL samples contained greater than 90% CLL B cells, as determined by fluorescence-activated cell sorter (FACS) analysis with anti-CD19, anti-CD5, and anti-CD23 monoclonal antibody (mAb). The murine stromal cell line M2-10B4 was obtained from the American Type Culture Collection (ATCC; Manassas, VA). Cells were maintained in RPMI 1640 medium containing 10% fetal calf serum (FCS) and penicillin-streptomycin-glutamine (Gibco BRL, Grand Island, NY) and were plated into 24-well plates at a concentration of 1.5×10^5 cells/well.

For experiments with NLCs, CLL cells were plated into 12-well plates at a concentration of 2×10^7 cells/well and were left for 14 days in culture to allow the adherent NLCs to spread out. After 14 days, CLL cells were removed from the NLCs, washed, and added back to the NLCs or, as controls, were put into fresh plates without NLCs, as described previously.[7]

Synthetic human CXCL12 was purchased from Upstate Biotechnology (Lake Placid, NY). The CXCR4 chemokine receptor antagonist T140, a 14-amino acid residue peptide,[16] and its analogs TC14012 and TN14003, which have higher stability in serum because they are C-terminally amidated,[15,16] were developed by us. Molecular weights of these compounds are approximately 2500. The highest concentration used in the experiments, 100 μg/mL, corresponds to 40 μM. The CXCR4 receptor antagonist AMD3100 was purchased from Sigma-Aldrich (Schnelldorf, Germany). Fludarabine was purchased from Medac Schering Onkologie (Munich, Germany) and was dephosphorylated with alkaline phosphatase (Gibco BRL) to the dephosphorylated nucleoside arabinosyl-2-fluoroadenine (F-ara-A) according to the protocol described by Huang and Plunkett.[17] Antibodies against phospho-p42/44, p42/44, phospho-signal transducer and activator of transcription 3 (phospho-STAT3), and STAT3 were purchased from Cell Signaling Technology (Beverly, MA).

For flow cytometry, the cells were analyzed on a FACScalibur (Becton Dickinson, Mountain View, CA). Flow cytometry data were analyzed using the FlowJo 3.3 software (Tree Star, San Carlos, CA).

Actin polymerization assay

Actin polymerization was tested as described.[18,19] Briefly, cells (1.25×10^6/mL) were suspended in RPMI 1640 medium with 0.5% bovine serum albumin (BSA) at 37°C and incubated with 100 ng/mL CXCL12. At the indicated time points, 400 μL cell suspension was added to 100 μL of a solution containing 4×10^{-7} M fluorescein isothiocyanate (FITC)–labeled phalloidin (Sigma-Aldrich), 0.5 mg/mL 1-α-lysophosphatidylcholine (Sigma-Aldrich, Germany), and 18% formaldehyde in phosphate-buffered saline (PBS). Fixed cells were analyzed by flow cytometry on a FACScalibur, and all time points were plotted relative to the mean fluorescence of the sample before chemokine was added.

Chemotaxis assay

CLL cells were suspended in RPMI 1640 with 0.5% BSA. For CXCR4 inhibition experiments, CLL cells were preincubated for 30 minutes with different concentrations of T140 before they were added to the inserts. A total of 100 μL, containing 5×10^5 cells, was added to the top chamber of a 6.5-mm diameter Transwell culture insert (Costar, Cambridge, MA) with a pore size of 5 μm. Filters then were transferred to wells containing medium with or without CXCL12. Chambers were incubated for 2 hours at 37°C in 5% CO_2. After this incubation, the cells in the lower chamber were suspended and divided into aliquots for counting with a FACScalibur for 20 seconds as described earlier.[13] Chemotaxis was expressed as the migration index, which was calculated according to the following formula: number of cells in the lower well/([number of cells in the lower well + number of cells in the upper chamber] × 100).

In vitro migration of CLL cells beneath stromal cells

Migration beneath stromal cells was performed as described previously.[13] Briefly, M2-10B4 stromal cells (ATCC) were seeded onto collagen-coated 24-well plates at a concentration of 1.5×10^5 cells/well in medium. After overnight culture, CLL cells were incubated with inhibitors for 30 minutes at room temperature and were added onto the confluent stromal cell layer to a final concentration of 5×10^6 cells/well. Plates were incubated at 37°C in 5% CO_2. After incubation for 4 to 6 hours, the cells that had not migrated to the stromal cell layer were removed by vigorous washing of the wells 3 times with RPMI 1640. The complete removal of nonmigrated cells and the integrity of the stromal cell layer containing transmigrated cells were assessed by phase-contrast microscopy and were documented photographically. Pseudoemperipolesis, the spontaneous migration of CLL cells beneath stromal cells, is characterized by the dark appearance of cells that have migrated to the same focal plane as the stromal cells, whereas the more superficial nonmigrated cells remain refractile. The stromal cell layer containing the migrated cells then was detached by incubation with trypsin/EDTA (ethylenediaminetetraacetic acid) solution (Gibco BRL) resuspended in 0.5 mL medium for counting by flow cytometry. A lymphocyte gate was set using the different relative size and granularity (forward scatter and side scatter) characteristics to exclude stromal cells. Duplicate samples were counted at high flow rates for 20 seconds to determine the relative number of migrated cells. A 1:20 diluted sample of supernatant cells resuspended to 0.5 mL was counted under the same conditions to determine the relative proportion of migrated cells.

Western blotting

For immunoblot analyses, 1×10^7 CLL cells were serum starved for 2 hours, treated with CXCL12 at 200 ng/mL for the indicated time points, and used to make lysates. Equal amounts of protein were separated by 10% sodium dodecyl sulfate–polyacrylamide gel electrophoresis (SDS-PAGE) and were transferred to polyvinylidene difluoride (PDVF) membranes. Immunoblot analysis was performed using p44/42, STAT3, phopho-p44/42, and phospho-STAT3 antibodies that specifically recognize the phosphorylated Thr202/Tyr204 of p44/42 MAPK protein and the phosphorylated serine (Ser727) of STAT3, respectively (Cell Signaling Technology). Immunoreactive bands were visualized using horseradish peroxidase–conjugated goat antirabbit secondary antibody and the enhanced chemiluminescence system (Amersham Biosciences, Freiburg, Germany).

Measurement of cell viability

Determination of CLL cell viability was based on the analysis of mitochondrial transmembrane potential by 3,3-dihexyloxocarbocyanine iodine ($DiOC_6$) and cell membrane permeability to propidium iodide (PI), as described.[20,21] For viability assays, 200 μL cell suspension was collected at the indicated time points and transferred to FACS tubes containing 200 μL of 60 nM $DiOC_6$ (Molecular Probes, Eugene, OR) and 10 μg/mL PI (Molecular Probes) in RPMI with 0.5% BSA. Cells were then incubated at 37°C for 15 minutes and analyzed within 30 minutes by flow cytometry using a FACScalibur (Becton Dickinson). Fluorescence was recorded at 525 nm (FL-1) for $DiOC_6$ and at 600 nm (FL-3) for PI.

Statistical analysis

Results are shown as mean plus or minus SD, or standard error of the mean (SEM), of at least 3 experiments each. For statistical comparison between groups, the Student paired *t* test or Bonferroni *t* test was used. Analyses were performed using the biostatistics software developed by Stanton A. Glantz (University of California at San Francisco). Flow cytometry data were analyzed using the FlowJo 3.3 software.

Results

T140 inhibits CXCL12-induced actin polymerization, chemotaxis, and pseudoemperipolesis in CLL B cells

Reorganization of the actin cytoskeleton is an early event in the migratory response to chemokines.[22] CXCL12 induces changes in the actin cytoskeleton of CLL cells.[13] Typically, a significant, transient increase in F-actin occurs within 15 seconds of exposure to CXCL12, followed by subsequent depolymerization. We examined whether this response to CXCL12 could be blocked by T140. As shown in Figure 1A, CXCL12-induced actin polymerization is inhibited in a dose-dependent manner. At higher concentrations (10 and 100 μg/mL), actin polymerization is completely abolished. Data shown are mean ± SEM of 9 experiments with CLL B cells from different patients.

Figure 1B depicts the inhibition of actin polymerization in response to CXCL12 by another CXCR4 antagonist, AMD3100, in comparison with T140. At a concentration of 4 μM AMD3100, actin polymerization was approximately 80% abolished, and at a concentration of 40 μM, the reaction was completely abolished. For comparison, we used 4 μM T140 (10 μg/mL), which completely abolished the reaction.

We also examined whether T140 could inhibit CXCL12-induced chemotaxis of CLL cells. As shown in Figure 1C, T140 inhibited chemotaxis relative to that of control cultures in a dose-dependent fashion, resulting in a 42.5% inhibition of chemotaxis at 100 ng/mL, 76% inhibition at 1 μg/mL, and greater than 80% inhibition at 10 μg/mL (4 μM; Figure 1C).

Coculture of CLL cells with marrow cells resulted in the spontaneous migration of CLL cells to the stromal cell layer (pseudoemperipolesis). We previously demonstrated that the CXCR4-CXCL12 interaction plays a key role for this migration phenomenon. To assess the efficacy of CXCR4 antagonists to inhibit this migration, pseudoemperipolesis of CLL cells was quantified by flow cytometry with or without preincubation of CLL cells with T140. We found that T140 inhibited pseudoemperipolesis in a dose-dependent manner (Figure 1D). Maximum inhibition of pseudoemperipolesis was achieved at concentrations of 1 μg/mL (0.4 μM). This inhibition of pseudoemperipolesis was confirmed by phase-contrast microscopy before detachment of the stromal layer for flow cytometry.

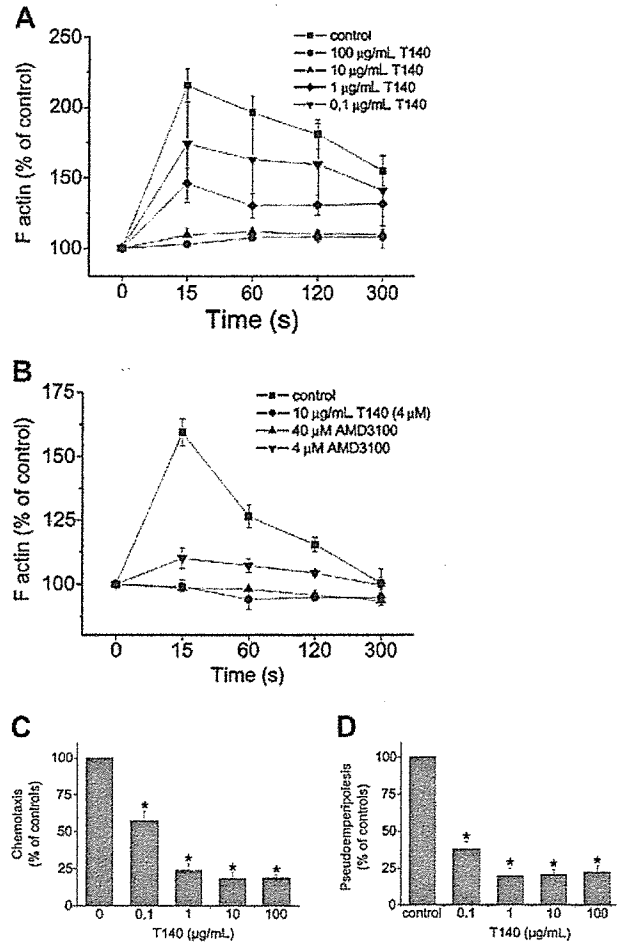

Figure 1. Inhibition of CXCL12-induced responses in CLL cells by T140 and AMD3100. (A) Actin polymerization of CLL cells in response to CXCL12 preincubated with different concentrations of T140. Intracellular F-actin in cells was measured using FITC-labeled phalloidin 15, 60, 120, and 300 seconds after the addition of 200 mg/mL CXCL12. Results are shown as percentages of intracellular F-actin relative to the values before the addition of CXCL12 and are mean ± SEM of 9 experiments. (B) Inhibition of actin polymerization of CLL cells in response to CXCL12 by the CXCR4 antagonists T140 and AMD3100. Cells were preincubated with 4 μM or 40 μM AMD3100 before stimulation with CXCL12. Inhibition of the response by 10 μg/mL T140 (4 μM) is shown for comparison. Results are displayed as percentages of intracellular F-actin relative to the values before the addition of CXCL12 and are the mean ± SEM of 4 CLL samples from different patients. (C) CXCL12-induced chemotaxis is inhibited by T140. Results indicate relative migration compared with control samples migrating to 200 ng/mL CXCL12 (100%) and samples preincubated with different concentrations of T140, representing the mean ± SEM values of 12 experiments with CLL cells from different patients (*$P < .05$). (D) In vitro migration of CLL cells beneath stromal cells (pseudoemperipolesis) is inhibited to T140. Cells were seeded onto M2-10B4 cells and allowed to migrate to the stromal cell layer. After vigorous washings, the remaining CLL cells were quantified using flow cytometry. Results are represented relative to untreated controls (100%). T140 was used at different concentrations, as indicated in the figure. Data shown are mean ± SEM values of 10 experiments with CLL cells from different patients (*$P < .05$).

TC14012 and TN14003 inhibit antiapoptotic effects of CXCL12 and marrow stromal cells

We examined whether T140 could inhibit the protective effect(s) of NLCs on CLL cells in vitro. As shown in Figure 2A, CLL cells that were grown on NLCs for 2 weeks and then reseeded into plates without NLCs lost approximately 20% viability within 48 hours compared with control cells reseeded on NLCs. Adding 500 ng/mL CXCL12 to the medium of CLL cells plated without NLCs increased CLL cell viability to almost the same viability as CLL cells seeded onto NLCs (94.4% ± 7.3% on day 1, 91.2% ± 5.1% on day 2, and 93.5% ± 10.7% on day 3 compared with a relative

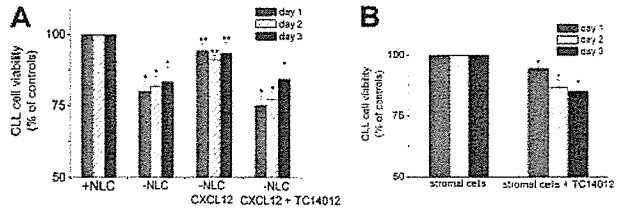

Figure 2. TC14012 inhibits protective effects of CXCL12 and accessory cells. (A) CLL cells were grown on NLCs for 2 weeks and then reseeded on the NLCs (controls; 100% viability) or seeded into wells without NLCs and treated with or without CXCL12 and with CXCL12 and TC14012 (100 μ/mL), as indicated. Presented are the mean ± SEM relative viabilities related to the viabilities of CLL cells remaining on NLCs of 10 experiments with cells from different CLL patients. CLL cells cultured without NLCs or without NLCs in the presence of CXCL12 and TC14012 had significantly reduced viability at each of the indicated time points (*$P < .05$). Synthetic CXCL12 partially restores the antiapoptotic effect of NLCs, resulting in a significantly higher viability of CLL cells without NLCs in the presence of synthetic CXCL12 (third block; **$P < .05$) when compared with CLL cells without NLCs (second block). (B) CLL cells were seeded onto M1-10B4 stromal cells with or without TC14012, and cell viability was measured after 24, 48, and 72 hours. Cell viability was related to the viability of M1-10B4 stromal cells (100%). Presented are the mean ± SEM relative viabilities related to the viabilities of CLL cells remaining on M2-10B4 cells of 8 experiments with cells from different patients (*$P < .05$).

viability of 100% for CLL cells cultured on NLCs). On the other hand, adding TC14012 to the CLL cells cultured in the presence of CXCL12 reduced the viability of CLL cells to 75.2% ± 3.7%, 77.1% ± 2.7%, and 84.2% ± 3.9% of the control cultures on days 1, 2, and 3, respectively. Similar results were obtained with TN14003 (64.6% ± 3.7%, 70.6% ± 3.0%, and 68.8% ± 5.8% viability on days 1, 2, and 3, respectively), which is comparable to the viability of CLL cells cultured without NLCs. Adding TC14012 to CLL cells cultured in the presence of NLCs induced only a minor decrease in viability of CLL cells (less than 5% decrease in viability compared with controls); however, this difference was not significant, possibly because of other NLC-associated antiapoptotic factors, as outlined under "Discussion."

In parallel, the inhibitors were added to CLL cells from 3 patients and to lymphocytes from 3 healthy volunteers to rule out toxic effects of the inhibitors. Treatment of CLL cells and lymphocytes with the same concentrations (0.1-100 μg/mL) of the inhibitors showed no toxic effect in comparison with untreated control cells on either of the cells on days 1, 2, and 3 (data not shown). The declining viability that occurs over time when CLL cells are cultured alone, as stated, was not affected by the addition of the inhibitors. Because mononuclear cells from patients showed differences in the presence and in the number of outgrowing NLCs, we subsequently focused on experiments with the stromal cell line M2-10B4. These cells constitutively secrete high amounts of CXCL12 and protect CLL cells from spontaneous apoptosis in a fashion similar to that for NLCs. CLL cells cultivated on M2-10B4 cells remained viable for a long period of time in culture. In addition, as shown in Figure 2B, adding the inhibitor TC14012 reduced the relative viability of CLL cells to 93.9% ± 0.8% on day 1, 86.2% ± 3.2% on day 2, and 84.9% ± 2.6% on day 3 compared with untreated controls.

T140, TC14012, and TN14003 inhibit CXCL12-induced p44/42 MAPK activation

We have previously shown that engagement of CXCR4 by CXCL12 in CLL cells induces robust, prolonged p42/44 MAPK signaling. Preincubation of CLL cells with the CXCR4 inhibitors T140, TC14012, and TN14003 before stimulation with CXCL12 completely abolished the phosphorylation of p42/44. Figure 3A shows a representative Western blot of 5 experiments with cells from different patients.

T140, TC14012, and TN14003 inhibit CXCL12-induced serine phosphorylation of STAT3 in cytosolic fractions

As described earlier, Ser727 of STAT3 is constitutively phosphorylated in CLL B cells.[23] We were able to show significant additional STAT3 phosphorylation on stimulation with 200 ng/mL CXCL12 for 10 minutes. As shown in Figure 3B, this CXCL12-induced phosphorylation could also be inhibited by all 3 inhibitors tested. Densitometry was performed to quantify the relative changes in phosphorylation of p42/44 MAPK and STAT3, and the data corresponding to the Western blots (Figure 3A-B) are displayed in Figure 3C.

Inhibition of protective effects of marrow stroma on CLL cells against drug-induced apoptosis

We treated CLL cells with different concentrations of F-ara-A (0.1, 1, 10, 50, and 100 μM), the dephosphorylated form of fludarabine, which is the most common chemotherapeutic treatment for CLL patients. CLL cells were plated with or without M2-10B4 cells, and cell viability was measured after 24, 48, and 72 hours of treatment. We found that M2-10B4 cells protected CLL cells from apoptosis at all drug concentrations tested. Data of one representative experiment with different concentrations of F-ara-A for 48 hours are displayed in Figure 4A. Figure 4B shows the protective effect of M2-10B4 cells on the survival of CLL cells treated with 10 μM F-ara-A for 24, 48, and 72 hours with or without stromal cells (99.6% ± 4% vs 97.8% ± 0.5%, 90.7% ± 1.8% vs 57.8% ± 5.5%, and 80.8 % ± 2.8% vs 20% ± 4.1% viability of the CLL cells; mean ±SEM; n = 10).

As shown in Figure 4C, a comparable protective effect was seen when CLL cells were treated with F-ara-A in the presence or absence of NLCs. After 48 hours of treatment with F-ara-A, the survival of CLL cells was significantly higher when cultured in the presence of NLCs.

To test whether the protective effect of M2-10B4 cells on chemotherapy-induced apoptosis can be abolished by the inhibitors, we compared the apoptosis of CLL cells treated with F-ara-A or with a combination of F-ara-A (10 μM) and TC14012 (100

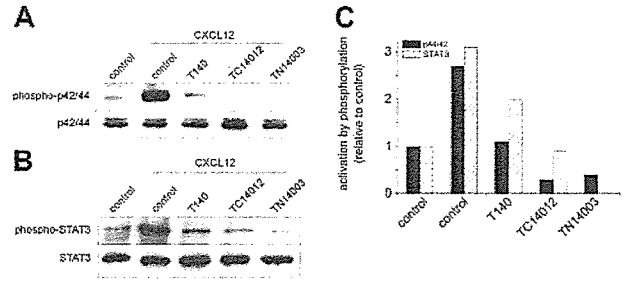

Figure 3. T140, TC14012, and TN14003 inhibit CXCL12-induced p42/44 MAPK activation and STAT3 serine phosphorylation. Cells were preincubated with 100 μg/mL T140, TC14012, and TN14003 for 30 minutes before stimulation with 200 ng/mL CXCL12 for 10 minutes. (A) Western blot analysis was performed on cell lysates with anti–phospho-p42/44 (top blot) and anti-p42/44 (bottom blot) antibodies. The blot shows representative results from 1 of 5 experiments with CLL B cells from different patients. (B) Western blot analysis was performed on cytosolic fractions with an antibody specific for serine phosphorylation of STAT3 (top blot). The bottom blot shows the membrane reprobed with an anti-STAT3 antibody. (C) Densitometry of the Western blots confirmed the reduction in p42/44 MAPK and STAT3 activation by preincubation with CXCR4 antagonists. Bars represent the phosphorylation of p42/44 MAPK and STAT3, as displayed in panels A and B after analysis by densitometry relative to the unstimulated controls (left-hand block).

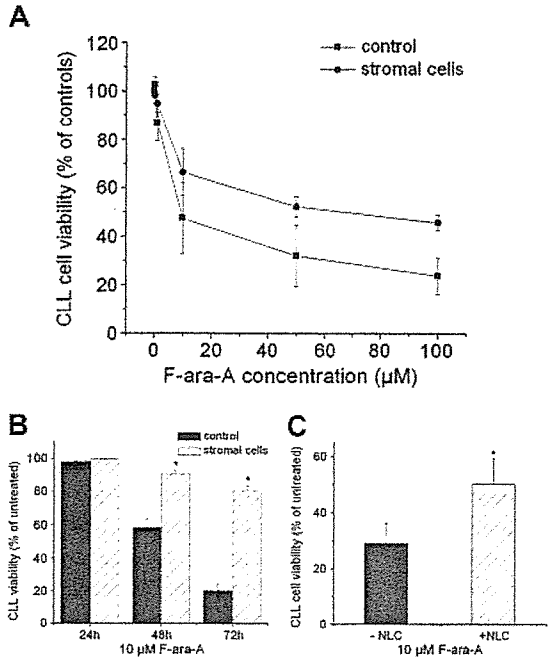

Figure 4. Marrow stromal cells and NLCs protect CLL cells against F-ara-A–induced apoptosis. (A-B) Cultivation on stromal cells protected CLL cells from F-ara-A–induced apoptosis. (A) CLL cell viability after 48-hour treatment with the indicated F-ara-A concentrations. Cells were cultivated with or without M2-10B4 stromal cells and treated with the indicated F-ara-A concentrations. CLL cell viability was determined after 48-hour treatment. Results are represented relative to untreated controls (100%) and are the mean ± SEM values of 4 different patients. (B) CLL cell viability with or without M2-10B4 stromal cells after 24-, 48-, and 72-hour treatment with 10 μM F-ara-A. Results are represented relative to untreated controls (100%) and are the mean ±SEM values of 10 patients. *Significant differences of CLL cell viability with stromal cells compared with CLL cell viability without stromal cells ($P < .05$). (C) NLCs protect CLL B cells against F-ara-A–induced apoptosis. CLL cells were grown in the presence of NLCs for 14 days and reseeded with or without NLCs before treatment with 10 μM F-ara-A. CLL cell viability was determined after 48 hours. Data are the mean ± SEM values of 6 patients (*$P < .05$).

μg/mL). Figure 5A displays FACS analysis of CLL cell viability of cells taken from a patient with CLL and cultivated with and without M2-10B4 cells and treated with 10 μM F-ara-A or a combination of F-ara-A and TN14003 72 hours after treatment. Whereas the addition of TN14003 to CLL cells cultured without stromal cells did not lead to a significant additional decrease in viability, the addition of TN14003 decreased the viability of cells cultured on stromal cells from 58% to 27% in this case. Figure 5B demonstrates the inhibitory effect of TN14003 on stromal cell–mediated protection of CLL cells from F-ara-A–induced apoptosis. CLL cells cultured on M2-10B4 cells treated with F-ara-A and TN14003 displayed a significant decrease in viability compared with CLL cells treated without TN14003 (80.6 % ± 3.3% vs 90.7% ± 1.8% and 68.3% ± 3.9% vs 80.8% ± 2.8% on days 2 and 3 respectively; mean ± SEM; n = 10; $P < .05$).

Discussion

Cell adhesion has been considered an important mechanism of primary drug resistance in malignant diseases such as acute and chronic leukemia, lymphoma, lung cancer, and breast cancer. Evidence is accumulating that interactions between CLL B cells and accessory cells confer a growth advantage, an extended cell survival, and drug resistance to chronic lymphoid tumors of B-cell type (for reviews, see Caligaris-Cappio[3] and Chiorazzi et al[4]). This mechanism of primary drug resistance has been termed cell adhesion–mediated drug resistance (CAM-DR).[24] Therefore, the identification of molecular targets that link malignant B cells to the microenvironment may lead to new therapeutic avenues for CLL patients.

In this study we demonstrate that small peptide inhibitors that specifically block the CXCR4 chemokine receptor inhibit the activation of CLL cells in response to stimulation with CXCL12 (SDF-1). Furthermore, CXCR4 receptor antagonists inhibit chemotaxis of CLL cells and their migration beneath marrow stromal cells (pseudoemperipolesis). To further investigate the effects of CXCR4 antagonists on CXCR4 downstream signaling events related to prosurvival or antiapoptotic effects, we tested for p42/44 MAPK activation and STAT3 phosphorylation. By pretreatment of CLL cells with T140 or its analogs, we were able to block almost completely the robust CXCL12-induced p42/44 phosphorylation, as displayed in Figure 3A. Another new finding in this study is that activation of the CXCR4 receptor results in the serine phosphorylation of STAT3 protein. STAT proteins are critical in mediating the response of hematopoietic cells to a diverse spectrum of cytokines. Frank et al[23] described constitutive serine phosphorylation in CLL samples, whereas Jurlander et al[25] described STAT3 activation in CLL B cells on interleukin-10 (IL-10) stimulation. As shown in Figure 3B, we noticed little constitutive STAT3 phosphorylation,

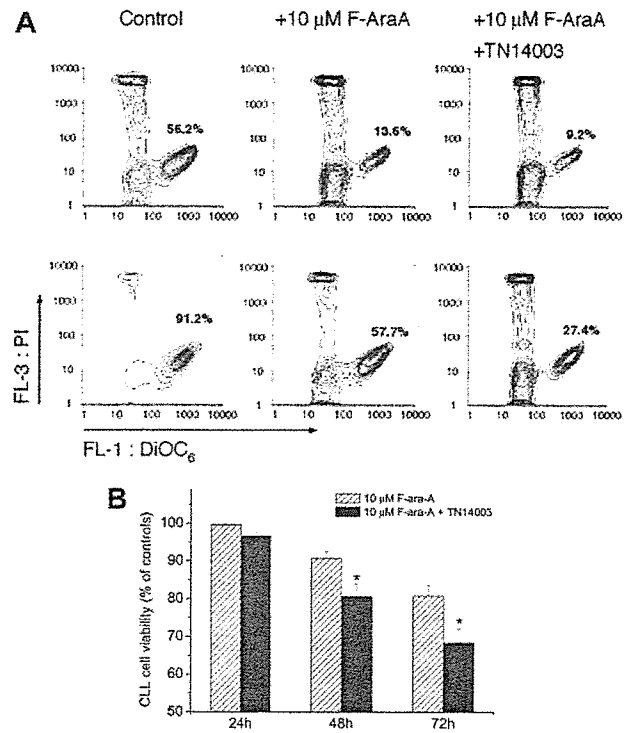

Figure 5. TN14003 antagonizes protective effects of marrow stromal cells. (A) Determination of cell viability by staining with $DiOC_6$ and PI. Presented are contour maps of CLL B cells from one patient defining the relative green ($DiOC_6$) and red (PI) fluorescence intensities of CLL cells on the horizontal and vertical axes, respectively. The vital cell population ($DiOC_6^{bright}$, $PI^{exclusion}$) was determined for CLL cells cultured in the presence (top row) or absence (bottom row) of M2-10B4 cells and 72 hours after treatment with 10 μM F-ara-A and TN14003. The percentage of vital cells is displayed in each contour map. (B) CLL cells were cultured on M2-10B4 stromal cells and treated with 10 μM F-ara-A or the combination of F-ara-A and 10 μg/mL TN14003. Cell viability was measured 24, 48, and 72 hours after treatment, as indicated on the horizontal axis. Data represent the mean relative viability of CLL cells treated with 10 μM F-ara-A (▨) or 10 μM F-ara-A and TN14003 (■) compared with the respective viability of CLL cells cultured on M2-10B4 stromal cells without F-ara-A or TN14003 (controls). Displayed are the mean ± SEM values of 10 patient samples (*$P < .05$).

but CXCL12 induced a strong serine phosphorylation of STAT3 protein. STAT proteins usually become activated on tyrosine and serine phosphorylation and are subsequently translocated from the cytosol to the nucleus, where they exert DNA-binding activity elements[26] and modulate the expression of target genes. As demonstrated in Figure 3B, the serine phosphorylation of CLL cells is completely inhibited by T140 and its analogs.

Although conventional tissue culture conditions result in a rapid decline in CLL cell viability (as outlined in the introduction), culture with stromal or nurselike cells protects CLL cells from apoptosis in vitro and thus appears to reflect interactions with the protective microenvironment in vivo. We found that this protective effect of stromal cells and partially of NLCs on the spontaneous apoptosis of CLL cells was antagonized by CXCR4 inhibitors. The antiapoptotic effect of marrow stromal cells was significantly reduced by CXCR4 antagonists (Figure 2B), whereas the effect of CXCR4 antagonists was lower in cocultures with NLCs and did not reach statistical significance. This difference may be attributed to several factors. First, the outgrowth and dependency of CLL cells on NLC support varies among patient samples, which makes the results heterogeneous (J.A.B., unpublished observations, January 1999). Moreover, NLCs express B-cell activating factor (BAFF) and a proliferation-inducing ligand (APRIL) belonging to the tumor necrosis factor (TNF) family that can protect CLL B cells from spontaneous apoptosis in a paracrine manner, as reported by Nishio et al.[27] Deaglio et al[28] recently reported that NCLs from patients with B-CLL also express CD31 and plexin-B1 (high-affinity CD100 ligand), which deliver additional growth or survival signals to CLL B cells.[28] These molecules protect CLL B cells by activating molecular pathways that are distinct from those activated by NLC-derived CXCL12.[27] Our initial observation that CXCL12 is a central molecule in NLC-mediated protection of CLL cells from apoptosis has been confirmed recently,[27] but the data discussed here indicate that NLC and CLL B cells are engaged in a complex molecular interaction that makes it more difficult to effectively block the antiapoptotic NLC effect with a single agent. Therefore, we decided to perform subsequent viability experiments with a supportive marrow stromal cell line with the advantages of consistent culture conditions along with a high constitutive CXCL12 secretion that protects CLL and other leukemia cells, as noted earlier by us and others.[10,14,29]

Comparable results with CXCR4 inhibitors have recently been described by Juarez et al[30] in acute lymphoblastic leukemia (ALL) cells. In a nonobese diabetes/severe combined immunodeficiency (NOD/SCID) mouse model of human high-grade NHL, CXCR4 neutralization by anti-CXCR4 mAbs had impressive efficacy without toxicity.[31]

Interestingly, we furthermore demonstrated that stromal cells protected CLL cells from fludarabine (F-ara-A)–induced apoptosis as an example of cell adhesion–mediated drug resistance. Treatment of CLL cells with CXCR4 receptor antagonists partially resensitized the CLL cells to F-ara-A, suggesting that treatment of CLL patients with such antagonists could mobilize CLL cells from protective microenvironments and make them more accessible to conventional therapy. The general feasibility and safety of such an approach has been demonstrated by recent studies in which CXCR4 antagonists were administered to patients or volunteers. Mobilization of hematopoietic progenitors in 26 healthy volunteers by the CXCR4 antagonist AMD3100 has recently been reported by Liles et al.[32] Single subcutaneous injection at doses up to 240 μg/kg per day induced rapid, generalized leukocytosis associated with a transient increase (up to 10-fold) in peripheral blood $CD34^+$ cells. Administration was well tolerated and produced only mild, transient toxicity. In addition, Devine et al[33] recently reported AMD3100 as a safe and effective agent for the mobilization of $CD34^+$ cells in patients with multiple myeloma and non-Hodgkin lymphoma who previously underwent chemotherapy. Premature ventricular contractions were observed in 2 of 40 HIV-infected patients in another clinical study with AMD3100, which resulted in the discontinuation of this trial.[34]

Several CXCR4 antagonists have been described, of which 2 (AMD3100 and ALX40-4C) have been administered to human subjects, as outlined here. Recent studies that compared the structural basis for the interaction of T140 and AMD3100 with CXCR4 demonstrated that the mechanisms used by these agents are different.[35,36] AMD3100 and ALX40-4C display weak, partial agonist (CXCL12-like) activity, whereas T140 has been characterized as an inverse agonist. Because agonist activity could be a disadvantage in treatment of diseases in which CXCR4 activation provides a survival signal (such as in CLL cells), T140-derived CXCR4 antagonists might have some advantage in clinical development compared with AMD3100 and ALX40-4C. Meanwhile, several animal studies have demonstrated the efficacy and safety of T140-derived CXCR4 antagonists that provide the basis for a clinical trial with these agents.[15,30,37-39]

However, the adhesive interactions between CLL cells and accessory cells and their protective effect on CLL cell survival was not completely abolished by the CXCR4 antagonists. The multistep paradigm of leukocyte activation by chemokines, initially described by Springer,[40] requires cooperation between integrin binding to their respective ligands along with chemokine receptor activation to sustain cell-cell adhesion. De la Fuente et al[41] demonstrated that adhesion of CLL B cells to the fibronectin fragment H89, a ligand for CD49d ($\alpha4\beta1$ integrins/VLA4), prevents their spontaneous apoptosis in vitro and that CLL B cells cultured on H89 during treatment with fludarabine showed significantly higher mean viability than cells cultured on control polylysine. We previously demonstrated that CLL B cells that migrate beneath marrow stromal cells displayed higher levels of CD49d than nonmigrated cells,[13] suggesting that $\alpha4\beta1$ integrin molecules indeed cooperate with CXCR4 receptors during CLL cell migration beneath marrow stromal cells. It is, therefore, likely that integrin-mediated survival signals may partially protect and compensate for CXCL12 survival signals in the direct culture system used here. Therefore, further studies will have to prove whether treatment with T140 analogs, along with integrin antagonists, synergize in inducing apoptosis in CLL cells.

In summary, this study demonstrates that the CXCR4 inhibitor T140 and its analogs effectively block all previously described functions of CXCL12 on CLL cells. Thereby, CXCR4 antagonists modulate biologically important functions of the leukemia cells that are essential for their localization and survival in a protective microenvironment. As such, a treatment concept that would first mobilize CLL cells from their protective microenvironment by using CXCR4 antagonists and then attack CLL B cells with cytotoxic agents such as fludarabine might increase the efficacy of current treatments. However, the mobilization of normal hematopoietic progenitor cells by CXCR4

antagonists is an important concern because the coadministration of a cytotoxic agent might increase the toxicity to normal hematopoiesis. B-cell targeted therapy, in combination with CXCR4 antagonists, could avert this potential hazard. Overall, our data suggest a potential role for CXCR4 antagonists in the treatment of B-cell CLL and also suggest that further in vivo investigation is warranted.

Acknowledgment

The authors thank Barbara Rogalsky for excellent technical assistance.

References

1. Keating MJ, Chiorazzi N, Messmer B, et al. Biology and treatment of chronic lymphocytic leukemia. Hematology (Am Soc Hematol Educ Program). 2003:153-175.
2. Munk Pedersen I, Reed J. Microenvironmental interactions and survival of CLL B-cells. Leuk Lymphoma. 2004;45:2365-2372.
3. Caligaris-Cappio F. Role of the microenvironment in chronic lymphocytic leukaemia. Br J Haematol. 2003;123:380-388.
4. Chiorazzi N, Rai KR, Ferrarini M. Chronic lymphocytic leukemia. N Engl J Med. 2005;352:804-815.
5. Han T, Barcos M, Emrich L, et al. Bone marrow infiltration patterns and their prognostic significance in chronic lymphocytic leukemia: correlations with clinical, immunologic, phenotypic, and cytogenetic data. J Clin Oncol. 1984;2:562-570.
6. Pangalis GA, Roussou PA, Kittas C, et al. Patterns of bone marrow involvement in chronic lymphocytic leukemia and small lymphocytic (well differentiated) non-Hodgkin's lymphoma: its clinical significance in relation to their differential diagnosis and prognosis. Cancer. 1984;54:702-708.
7. Lagneaux L, Delforge A, Bron D, De Bruyn C, Stryckmans P. Chronic lymphocytic leukemic B cells but not normal B cells are rescued from apoptosis by contact with normal bone marrow stromal cells. Blood. 1998;91:2387-2396.
8. Dorshkind K. Regulation of hemopoiesis by bone marrow stromal cells and their products. Annu Rev Immunol. 1990;8:111-137.
9. Panayiotidis P, Jones D, Ganeshaguru K, Foroni L, Hoffbrand AV. Human bone marrow stromal cells prevent apoptosis and support the survival of chronic lymphocytic leukaemia cells in vitro. Br J Haematol. 1996;92:97-103.
10. Burger JA, Tsukada N, Burger M, Zvaifler NJ, Dell'Aquila M, Kipps TJ. Blood-derived nurse-like cells protect chronic lymphocytic leukemia B cells from spontaneous apoptosis through stromal cell-derived factor-1. Blood. 2000;96:2655-2663.
11. Tsukada N, Burger JA, Zvaifler NJ, Kipps TJ. Distinctive features of "nurselike" cells that differentiate in the context of chronic lymphocytic leukemia. Blood. 2002;99:1030-1037.
12. Tashiro K, Tada H, Heilker R, Shirozu M, Nakano T, Honjo T. Signal sequence trap: a cloning strategy for secreted proteins and type I membrane proteins. Science. 1993;261:600-603.
13. Burger JA, Burger M, Kipps TJ. Chronic lymphocytic leukemia B cells express functional CXCR4 chemokine receptors that mediate spontaneous migration beneath bone marrow stromal cells. Blood. 1999;94:3658-3667.
14. Nishii K, Katayama N, Miwa H, et al. Survival of human leukaemic B-cell precursors is supported by stromal cells and cytokines: association with the expression of bcl-2 protein. Br J Haematol. 1999;105:701-710.
15. Fujii N, Nakashima H, Tamamura H. The therapeutic potential of CXCR4 antagonists in the treatment of HIV. Expert Opin Investig Drugs. 2003;12:185-195.
16. Tamamura H, Omagari A, Hiramatsu K, et al. Development of specific CXCR4 inhibitors possessing high selectivity indexes as well as complete stability in serum based on an anti-HIV peptide T140. Bioorg Med Chem Lett. 2001;11:1897-1902.
17. Huang P, Plunkett W. Action of 9-beta-D-arabinofuranosyl-2-fluoroadenine on RNA metabolism. Mol Pharmacol. 1991;39:449-455.
18. Bleul CC, Fuhlbrigge RC, Casasnovas JM, Aiuti A, Springer TA. A highly efficacious lymphocyte chemoattractant, stromal cell-derived factor 1 (SDF-1). J Exp Med. 1996;184:1101-1109.
19. Wulf E, Deboben A, Bautz FA, Faulstich H, Wieland T. Fluorescent phallotoxin, a tool for the visualization of cellular actin. Proc Natl Acad Sci U S A. 1979;76:4498-4502.
20. Dutt P, Wang JF, Groopman JE. Stromal cell-derived factor-1 alpha and stem cell factor/kit ligand share signaling pathways in hemopoietic progenitors: a potential mechanism for cooperative induction of chemotaxis. J Immunol. 1998; 161:3652-3658.
21. Ganju RK, Brubaker SA, Meyer J, et al. The alpha-chemokine, stromal cell-derived factor-1alpha, binds to the transmembrane G-protein-coupled CXCR-4 receptor and activates multiple signal transduction pathways. J Biol Chem. 1998; 273:23169-23175.
22. Baggiolini M. Chemokines and leukocyte traffic. Nature. 1998;392:565-568.
23. Frank DA, Mahajan S, Ritz J. B lymphocytes from patients with chronic lymphocytic leukemia contain signal transducer and activator of transcription (STAT) 1 and STAT3 constitutively phosphorylated on serine residues. J Clin Invest. 1997; 100:3140-3148.
24. Damiano JS, Cress AE, Hazlehurst LA, Shtil AA, Dalton WS. Cell adhesion mediated drug resistance (CAM-DR): role of integrins and resistance to apoptosis in human myeloma cell lines. Blood. 1999;93:1658-1667.
25. Jurlander J, Lai CF, Tan J, et al. Characterization of interleukin-10 receptor expression on B-cell chronic lymphocytic leukemia cells. Blood. 1997; 89:4146-4152.
26. Shuai K, Ziemiecki A, Wilks AF, et al. Polypeptide signalling to the nucleus through tyrosine phosphorylation of Jak and Stat proteins. Nature. 1993;366:580-583.
27. Nishio M, Endo T, Tsukada N, et al. Nurselike cells express BAFF and APRIL, which can promote survival of chronic lymphocytic leukemia cells via a paracrine pathway distinct from that of SDF-1α. Blood. Prepublished on April 28, 2005, as DOI 10.1182/blood-2004-04-0889.
28. Deaglio S, Vaisitti T, Bergui L, et al. CD38 and CD100 lead a network of surface receptors relaying positive signals for B-CLL growth and survival. Blood. 2005;105:3042-3050.
29. Lagneaux L, Delforge A, Massy M, Bernier M, Bron D. Increased production of SDF-1 by bone marrow (BM) stromal cells (SC) derived from chronic lymphocytic leukemia (CLL) patients in comparison with normal subjects : role in the migration of CLL B cells [abstract]. Blood. 2000;96: 362a.
30. Juarez J, Bradstock KF, Gottlieb DJ, Bendall LJ. Effects of inhibitors of the chemokine receptor CXCR4 on acute lymphoblastic leukemia cells in vitro. Leukemia. 2003;17:1294-1300.
31. Burger JA, Kipps TJ. Chemokine receptors and stromal cells in the homing and homeostasis of chronic lymphocytic leukemia B cells. Leuk Lymphoma. 2002;43:461-466.
32. Liles WC, Broxmeyer HE, Rodger E, et al. Mobilization of hematopoietic progenitor cells in healthy volunteers by AMD3100, a CXCR4 antagonist. Blood. 2003;102:2728-2730.
33. Devine SM, Flomenberg N, Vesole DH, et al. Rapid mobilization of CD34+ cells following administration of the CXCR4 antagonist AMD3100 to patients with multiple myeloma and non-Hodgkin's lymphoma. J Clin Oncol. 2004;22: 1095-1102.
34. Hendrix CW, Flexner C, MacFarland RT, et al. Pharmacokinetics and safety of AMD-3100, a novel antagonist of the CXCR-4 chemokine receptor, in human volunteers. Antimicrob Agents Chemother. 2000;44:1667-1673.
35. Trent JO, Wang ZX, Murray JL, et al. Lipid bilayer simulations of CXCR4 with inverse agonists and weak partial agonists. J Biol Chem. 2003;278: 47136-47144.
36. Zhang WB, Navenot JM, Haribabu B, et al. A point mutation that confers constitutive activity to CXCR4 reveals that T140 is an inverse agonist and that AMD3100 and ALX40–4C are weak partial agonists. J Biol Chem. 2002;277:24515-24521.
37. Takenaga M, Tamamura H, Hiramatsu K, et al. A single treatment with microcapsules containing a CXCR4 antagonist suppresses pulmonary metastasis of murine melanoma. Biochem Biophys Res Commun. 2004;320:226-232.
38. Mason DY, Andre P, Bensussan A, et al. CD antigens 2001. Tissue Antigens. 2001;58:425-430.
39. Murakami T, Maki W, Cardones AR, et al. Expression of CXC chemokine receptor-4 enhances the pulmonary metastatic potential of murine B16 melanoma cells. Cancer Res. 2002;62:7328-7334.
40. Springer TA. Traffic signals for lymphocyte recirculation and leukocyte emigration: the multistep paradigm. Cell. 1994;76:301-314.
41. de la Fuente MT, Casanova B, Garcia-Gila M, Silva A, Garcia-Pardo A. Fibronectin interaction with α4β1 integrin prevents apoptosis in B cell chronic lymphocytic leukemia: correlation with Bcl-2 and Bax. Leukemia. 1999;13:266-274.

Identification of Novel Low Molecular Weight CXCR4 Antagonists by Structural Tuning of Cyclic Tetrapeptide Scaffolds

Hirokazu Tamamura,*,⊥,# Takanobu Araki,⊥ Satoshi Ueda,⊥ Zixuan Wang,§ Shinya Oishi,⊥ Ai Esaka,⊥ John O. Trent,‖ Hideki Nakashima,† Naoki Yamamoto,‡ Stephen C. Peiper,§ Akira Otaka,⊥ and Nobutaka Fujii*,⊥

Graduate School of Pharmaceutical Sciences, Kyoto University, Sakyo-ku, Kyoto 606-8501, Japan; Institute of Biomaterials and Bioengineering, Tokyo Medical and Dental University, Chiyoda-ku Tokyo 101-0062, Japan; Medical College of Georgia, Augusta, Georgia 30912; James Graham Brown Cancer Center, University of Louisville, Louisville, Kentucky 40202; St. Marianna University, School of Medicine, Miyamae-ku, Kawasaki 216-8511, Japan; and Tokyo Medical and Dental University, School of Medicine, Bunkyo-ku, Tokyo 113-8519, Japan

Received January 5, 2005

A highly potent CXCR4 antagonist, compound **2**, was previously found by using two orthogonal cyclic pentapeptide libraries involving conformation-based and sequence-based libraries based on the pharmacophore of a 14-mer peptidic antagonist, **1**. Herein, cyclic tetrapeptides derived from replacements of the dipeptide unit (Nal-Gly) with a γ-amino acid and pseudopeptides cyclized by disulfide and olefin bridges were synthesized to find novel scaffold structures different from that of cyclic pentapeptides. These compounds contain a reduced number of peptide bonds compared to compound **2**. Furthermore, several analogues with chemical modification of the side chain of Arg^4 in **2** were also prepared. From these, several new leads possessing high to moderate CXCR4-antagonistic activity were characterized.

Introduction

The chemokine receptor, CXCR4, is a seven transmembrane (7TM) GPCR that transduces signals of its endogenous ligand, stromal cell-derived factor-1 (SDF-1).[1−4] The SDF-1/CXCR4 system plays an important role in the migration of progenitors during embryologic development of the cardiovascular, hemopoietic, and central nervous systems. Recently, this system has been shown to be involved in several diseases, including HIV infection,[5] cancer metastasis/progression,[6−20] and rheumatoid arthritis (RA).[21] CXCR4 was initially identified as a coreceptor that is utilized in T cell line-tropic (X4-) HIV-1 entry.[5] Müller et al. reported that CXCR4 and another chemokine receptor, CCR7, are highly expressed in human breast cancer cells, while SDF-1 and a CCR7 ligand, CCL21, are highly expressed in lymph nodes, bone marrow, lung, and liver, which represent the primary metastatic destinations of breast cancer, suggesting that the SDF-1/CXCR4 system might determine the metastatic destination of tumor cells.[6] Recently, this system has been recognized to be involved in the metastasis of several types of cancers, such as pancreatic cancer,[7,8] melanoma,[6,9] prostate cancer,[10] kidney cancer,[11] neuroblastoma,[12] non-Hodgkin's lymphoma,[13] lung cancer,[14] ovarian cancer,[15,16] multiple myeloma,[17] chronic lymphocytic leukemia,[18] acute lymphoblastic leukemia,[19] and malignant brain tumor.[20] Nanki et al. reported that the memory T cells highly express CXCR4 and the SDF-1 concentration is extremely high in the synovium of RA patients, and that SDF-1 stimulates migration of the memory T cells and inhibits T cell apoptosis, indicating that the SDF−CXCR4 interaction plays a critical role in T cell accumulation in the RA synovium.[21] Thus, CXCR4 is thought to be an important therapeutic target for these diseases. Compound **1** and its analogues, 14-mer peptides, were previously found to be specific CXCR4 antagonists that were characterized as HIV-entry inhibitors,[22] anticancer-metastatic agents[8,23] and anti-RA agents.[24] Arg^2, L-3-(2-naphthyl)alanine (Nal)[3], Tyr^5, and Arg^{14} were proven to constitute the critical pharmacophores of **1** (Figure 1).[25] The efficient utilization of two orthogonal cyclic pentapeptide libraries consisting of conformation-based and sequence-based libraries involving the critical residues of **1** led to molecular-size reduction of **1** and discovery of cyclic pentapeptides, **2** and **3**, which have strong CXCR4-antagonistic activity, comparable to that of **1**.[26] In this paper, we describe the fine-tuning of ring structures based on cyclic pentapeptide templates,[27−34] and chemical modifications of side chains for an increase in potency and a reduction of the peptide characteristics of **2**.[35]

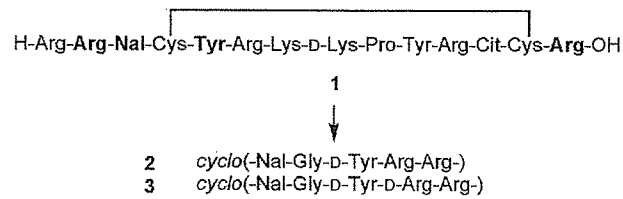

Figure 1. Reduction of the molecular size of a peptide **1** to cyclic pentapeptides **2** and **3**. Bold residues are the indispensable residues of **1** for the expression of strong CXCR4-antagonistic activity.

Chemistry

γ-Amino Acid-Containing Cyclic Tetrapeptides (11a−d). Requisite N^{γ}-Fmoc-γ-amino acids, (2*E*,4*S*)-N^{γ}-

* Corresponding authors. Tel: +81 75 753 4551, Fax: +81 75 753 4570, e-mail: tamamura@pharm.kyoto-u.ac.jp and nfujii@pharm.kyoto-u.ac.jp.
⊥ Kyoto University.
Institute of Biomaterials and Bioengineering.
§ Medical College of Georgia.
‖ University of Louisville.
† St. Marianna University.
‡ School of Medicine.

10.1021/jm050009h CCC: $30.25
Published on Web 04/13/2005

Scheme 1[a]

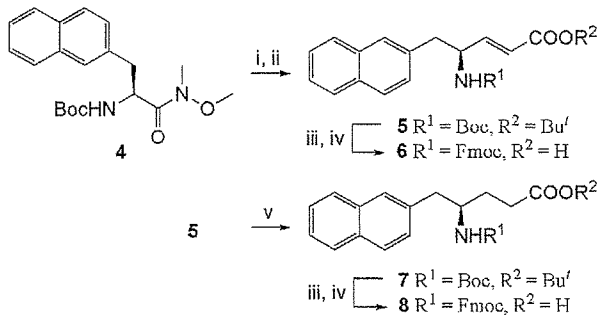

[a] Reagents: (i) DIBAL-H; (ii) $(EtO)_2P(O)CH_2CO_2Bu^t$,LiCl, DIPEA; (iii) 95% aqueous TFA; (iv) Fmoc-OSu, Et_3N; (v) H_2, Pd/C.

Scheme 2[a]

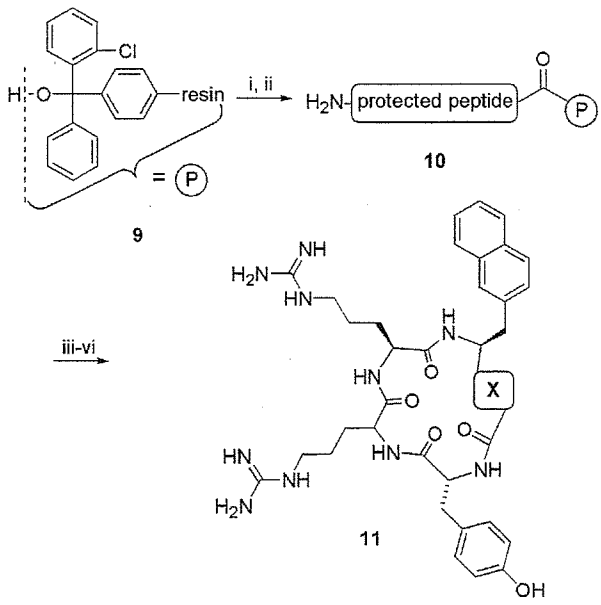

Compd.	Sequence (*cyclo*)	X
11a	(-γ-Nal[1]-D-Tyr[2]-D-Arg[3]-Arg[4]-)	-CH_2-CH_2-
11b	(-γ-Nal[1]-D-Tyr[2]-Arg[3]-Arg[4]-)	-CH_2-CH_2-
11c	(-γ-(*E*)-Nal[1]-D-Tyr[2]-D-Arg[3]-Arg[4]-)	-CH=CH-
11d	(-γ-(*E*)-Nal[1]-D-Tyr[2]-Arg[3]-Arg[4]-)	-CH=CH-

[a] Reagents: (i) **6** or **8**, DIPEA, DMF/CH_2Cl_2; (ii) Fmoc-based SPPS; (iii) AcOH/TFE/CH_2Cl_2; (iv) DPPA, $NaHCO_3$; (v) basic alumina column; (vi) 95% aqueous TFA.

Fmoc-4-amino-5-naphthalen-2-yl-pent-2-enoic acid (γ-(*E*)-Nal) **6** and (4*R*)-*N*γ-Fmoc-4-amino-5-naphthalen-2-yl-pentanoic acid (γ-Nal) **8**, were synthesized according to Scheme 1. Boc-Nal-NMe(OMe) **4** was treated with DIBAL followed by modified Horner–Wadsworth–Emmons olefination to yield Boc-γ-(*E*)-Nal-OBu^t **5**. *N*α-Fmoc-protection after the cleavage of the *N*α-Boc and Bu^t groups of **5** with TFA afforded a desired compound, Fmoc-γ-(*E*)-Nal-OH **6**. Hydrogenation of **5** obtained a reduced compound, **7**, which was similarly converted to another desired compound, Fmoc-γ-Nal-OH **8**. The protected peptide resin **10** was constructed by general Fmoc-based solid-phase synthesis on a (2-chloro)trityl resin **9**, in which the above γ-amino acid, **6** or **8**, was introduced as a C-terminal residue by DIPEA in DMF/CH_2Cl_2 (Scheme 2). Cleavage of the liner peptide from the resin with AcOH/TFE/CH_2Cl_2 (1:1:3 (v/v)) followed by cyclization with diphenylphosphoryl azide (DPPA)

Scheme 3[a]

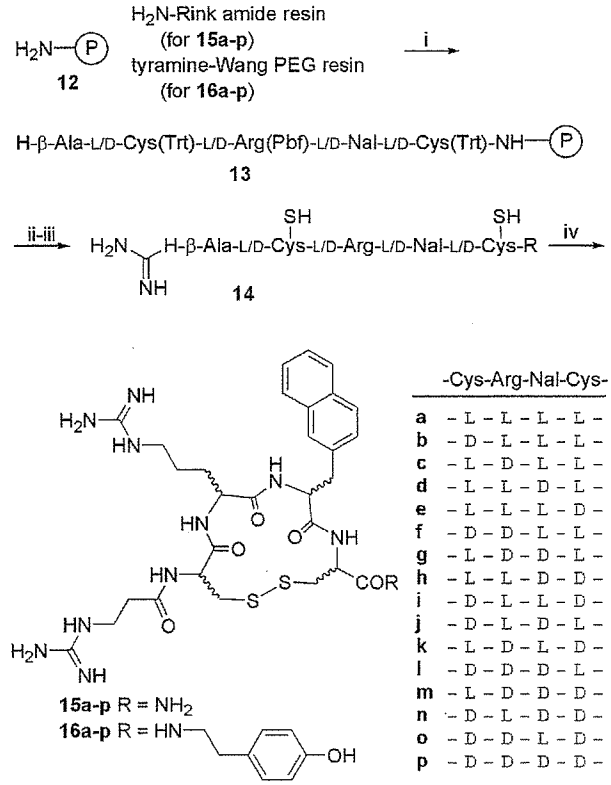

[a] Reagents: (i) Fmoc-based SPPS; (ii) 1*H*-pyrazole-1-carboxamidine hydrochloride, DIPEA; (iii) EDT/H_2O/TFA; (iv) aqueous $AcONH_4$ pH 8.

and $NaHCO_3$, subsequent deprotection with TFA and HPLC purification gave the desired cyclic peptide **11**.[26]

Disulfide-Bridged Cyclic Peptides (15a–p and 16a–p). The protected peptide resin was constructed by general Fmoc-based solid-phase synthesis on an NH_2-Rink amide resin (for **15a–p**) or a tyramine-Wang PEG resin (for **16a–p**) **12** (Scheme 3). Fmoc-β-Ala-OH was condensed to the N-terminus of the protected resin as the final residue. After deprotection of the Fmoc group, N-guanylation of the resulting free β-amino group with 1*H*-pyrazole-1-carboxamidine hydrochloride and DIPEA, followed by cleavage from the resin and removal of the 2,2,4,6,7-pentamethyldihydrobenzofuran-5-sulfonyl (Pbf) and Trt groups with EDT/H_2O/TFA, gave the crude reduced peptide (2SH-peptide) **14**. Subsequent air-oxidation of the crude 2SH-peptide **14** and HPLC purification yielded the desired disulfide peptide **15** or **16**.

Disulfide-Bridged Cyclic Peptides (15q and 16q). The protected peptide resin was constructed on an Fmoc-NH-Rink amide resin (for **15q**) or an Fmoc-tyramine-Wang PEG resin (for **16q**) in the same manner as in the synthesis of **15e** or **16e** (Table 1). Reductive amination of the N-terminal amino group of the protected resin with *N*-Fmoc-3-aminopropanal and $NaBH(OAc)_3$,[36] followed by removal of the Fmoc group and the subsequent N-guanylation of the resulting free amino group in the same manner as in the synthesis of **15e** or **16e**, obtained the protected pseudo-peptide resin. Cleavage from the resin and removal of the Pbf and Trt groups, the subsequent air-oxidation, and HPLC purification were performed in the same manner as in the

Table 1. Inhibitory Activity of Disulfide/Olefin-Bridged Cyclic Peptides against SDF-1 Binding to CXCR4

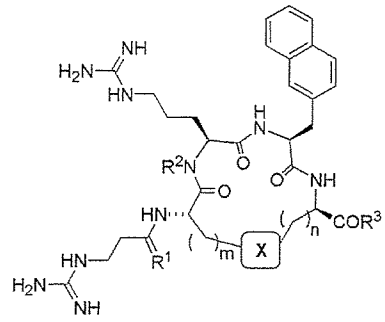

compd	m	n	X	R^1	R^2	R^3	$IC_{50} \pm SD$ (μM)[a]
15e	1	1	S–S	O	H	NH_2	0.69 ± 0.40
16e	1	1	S–S	O	H	tyramine	0.53 ± 0.28
15q	1	1	S–S	H_2	H	NH_2	ca. 1
16q	1	1	S–S	H_2	H	tyramine	ca. 1
15r	1	1	S–S	O	Me	NH_2	>10
16r	1	1	S–S	O	Me	tyramine	>10
20a	1	1	(*E*)-CH=CH	O	H	NH_2	1–10
20b	1	2	(*E*)-CH=CH	O	H	NH_2	1–10
20c	2	2	(*E*)-CH=CH	O	H	NH_2	1–10
20d	1	1	(*E*)-CH=CH	O	H	tyramine	1–10
2							0.0043 ± 0.0012
3							0.0084 ± 0.0038

[a] IC_{50} values are based on the inhibition of [^{125}I]-SDF-1 binding to CXCR4 transfectants of CHO cells. All data with standard deviation (SD) are the mean values for at least three independent experiments.

synthesis of **15e** or **16e** to yield the desired pseudopeptide, **15q** or **16q**.

Disulfide-bridged Cyclic Peptides (15r and 16r). The protected peptide resin was constructed on an Fmoc-NH-Rink amide resin (for **15r**) or an Fmoc-tyramine-Wang PEG resin (for **16r**) (Table 1). N^{α}-Methylation of the Arg(Pbf) residue in the protected resin was performed by the Fukuyama–Mitsunobu reaction.[37] N^{α}-*o*-Nitrobenzenesulfonyl (Ns) protection of H-Arg(Pbf)-Nal-D-Cys-NH-Rink amide (or -tyramine-Wang PEG) resin and the subsequent N^{α}-methylation with MeOH, Ph_3P, and diethyl azodicarboxylate (DEAD) were followed by removal of the N^{α}-Ns group with DBU and 2-mercaptoethanol. The next residue Fmoc-D-Tyr(Bu^t)-OH was condensed to the secondary N^{α}-amino group of the MeArg(Pbf) residue on the protected resin by using HATU, HOAt, and DIPEA. N-Guanylation, cleavage, deprotection, air-oxidation, and HPLC purification were subjected to yield the desired peptide, **15r** or **16r**.

Olefin-Bridged Cyclic Peptides (20a–d). The protected peptide resin was constructed on an NH_2-Rink amide resin (for **20a–c**) or an Fmoc-tyramine-Wang PEG resin (for **20d**) (Scheme 4) **12**. D-2-Allylglycine[38] (for **20a** or **20d**) or Fmoc-D-2-homoallylglycine[39,40] (for **20b** or **20c**) was used as the C-terminal residue, while Fmoc-L-2-allylglycine[41] (for **20a**, **20b**, or **20d**) or Fmoc-L-2-homoallylglycine[42] (for **20c**) was used as the N-terminal second residue. Fmoc-β-Ala-OH was condensed to the N-terminus of the protected resin as the final residue. The protected peptide resin **17** was subjected to ring-closing olefin metathesis with Grubbs catalyst second generation[43] to give the cyclized peptide resin **18**. After deprotection of the Fmoc group, N-guanylation of the resulting free β-amino group, followed by treatment with 1 M TMSBr-thioanisole/TFA and HPLC purification, gave the desired peptide **20**. The *E* geometry of the olefin units in **20a–d** was easily established from the coupling constants (J = 15.5, 15.6, 15.2, and 15.2 Hz, respectively) of the two olefinic protons by ^{1}H NMR analysis.

Scheme 4[a]

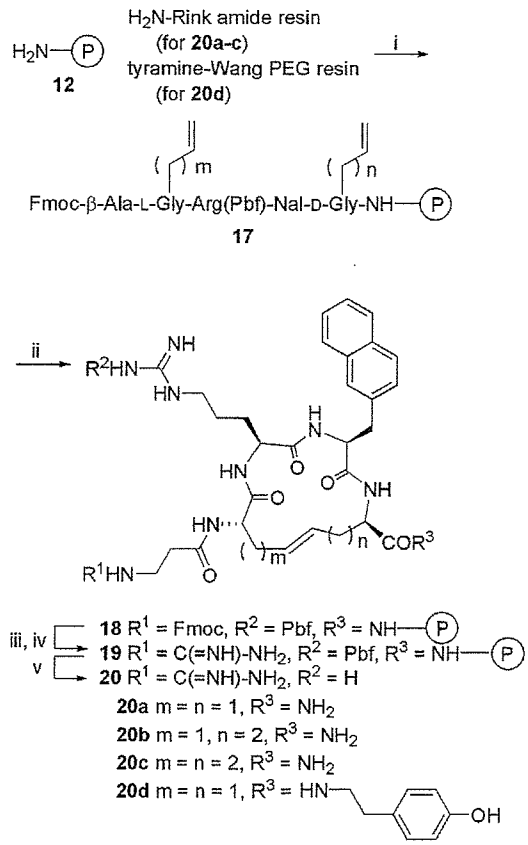

[a] Reagents: (i) Fmoc-based SPPS; (ii) Grubbs catalyst 2nd generation, (iii) piperdine; (iv) 1*H*-pyrazole-1-carboxamidine hydrochloride, DIPEA; (v) 1 M TMSBr-thioanisole/TFA.

Analogues with Substitution for Arg^4 (23a–p). Each peptide was synthesized in a general manner similar to that in the synthesis of **11a**. **23d** and **23f**: N^{α}-Methylation and coupling reaction to the N^{α}-methylated residue were performed in a manner similar to that in the synthesis of **15r**. **23j,k** and **23o,p**: After cyclization and deprotection, N-guanylation of the resulting free γ- or ϵ-amino group of the L-2,4-diaminobutyric acid (Dab)^4 or Lys^4 residue (for **23j** or **23k**, respectively) was performed with 1*H*-pyrazole-1-carboxamidine hydrochloride and DIPEA (Scheme 5). N-Guanylation of the resulting free γ-amino group of the *trans*- or *cis*-4-aminoproline residue[44] (for **23o** or **23p**, respectively) was similarly performed.

Biological Results and Discussion

γ-Amino Acid-Containing Cyclic Tetrapeptides. Cyclic pentapeptides, **2** and **3**, have a Gly residue as a spacer for cyclization. To reduce the ring size, the Nal-Gly sequences of **2** and **3** were replaced by a γ-Nal or γ-(*E*)-Nal unit (Scheme 2). Among these γ-amino acid-containing cyclic tetrapeptides (**11a–d**), only **11a** [substitution of γ-Nal for Nal-Gly of **3**] showed high CXCR4-antagonistic activity (IC_{50} = 54 nM) (Figure 2), although

Scheme 5[a]

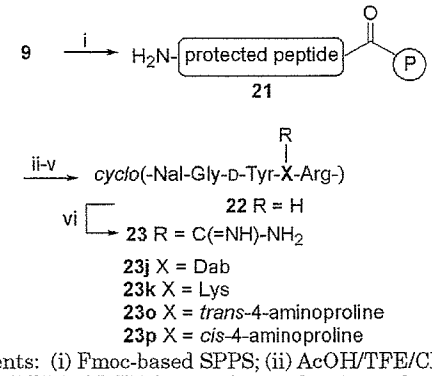

[a] Reagents: (i) Fmoc-based SPPS; (ii) AcOH/TFE/CH_2Cl_2 (1:1:3 (v/v)); (iii) DPPA, $NaHCO_3$; (iv) basic alumina column; (v) 95% aqueous TFA; (vi) 1*H*-pyrazole-1-carboxamidine hydrochloride, DIPEA.

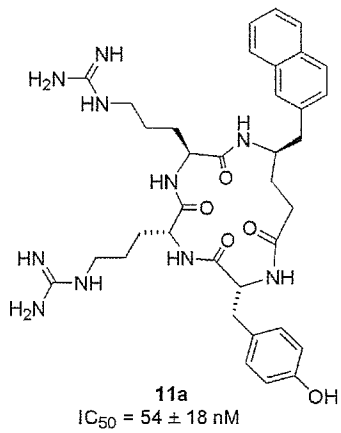

Figure 2. The structure of **11a**.

this activity is 6-fold lower than that of **3**. This result suggested that the Gly residue and the amide bond of the Nal-Gly sequence are not necessary for high activity. The reason for no significant activity of **11b** [substitution of γ-Nal for Nal-Gly of **2**] (IC_{50} > 1 μM) cannot be well explained, however, the difference of chirality of L/D-Arg^3 in **2** and **3** might cause a global conformational change of the ring. Both γ-(*E*)-Nal-substituted analogues, **11c** and **11d**, showed no significant activity (IC_{50} > 1 μM), suggesting that constraint of the γ-amino acid to the *E*-form might not be suitable.

Disulfide-Bridged Cyclic Peptides. To optimize the ring structures of compound **2**-derived compounds, the use of scaffold templates different from that of cyclic pentapeptides was investigated. Since the four requisite residues of **1** are disposed in close vicinity each other due to the disulfide bridge [Cys^4-Cys^{13}][45] and cyclic peptides possessing the Arg-Arg-Nal sequence, such as **2** and **3**, showed high CXCR4-antagonistic activity, we designed and separately prepared disulfide-bridged cyclic peptide libraries consisting of the *N*-3-guanidinopropanoyl-L/D-Cys(S-)-L/D-Arg-L/D-Nal-L/D-Cys-(S-)-NH_2 (or −tyramine) sequence, which included 32 compounds (2 × 2^4 stereoisomers) (**15a−p** or **16a−p**, respectively, Scheme 3). Among these synthetic compounds, **15e** [*N*-3-guanidinopropanoyl-Cys(S-)-Arg-Nal-D-Cys(S-)-NH_2] and **16e** [*N*-3-guanidinopropanoyl-Cys-(S-)-Arg-Nal-D-Cys(S-)-tyramine] exhibited moderate CXCR4-antagonistic activity (IC_{50} = 690 and 530 nM, respectively) (Table 1), although the other compounds did not show any activity up to the concentration of 1 μM. **15e** and **16e** have a common combination of chiralities of composed amino acids, suggesting that these compounds form similar conformations. It seems that a phenol group of **16e** is not disposed in the suitable position, since **15e** and **16e** have almost the same potencies. However, notably, L,L-chiralities of Arg-Nal are critical for high activity, as shown in **2** and **3**. The synthetic Arg side chain involving an *N*-3-guanidinopropanoyl moiety has an extra atom, compared to the original Arg side chain. This might account for the lower activity.

In addition, **15e/16e** analogues, **15q** and **16q**, in which the amide bond of *N*-3-guanidinopropanoyl-Cys was replaced by a reduced amide bond, and **15r** and **16r**, in which the α-amino group of Arg was N-methylated, were prepared. Substitution of the reduced amide bond for the amide bond of *N*-3-guanidinopropanoyl-Cys brought about no significant difference in potency (IC_{50} of **15q** and **16q** = c.a. 1 μM). This suggested that the planar character of this amide bond and the carbonyl group have little effect on potency. N-Methylation of Arg caused remarkable decrease in potency (IC_{50} of **15r** and **16r** > 10 μM), indicating that conformation surrounded by the Cys-Arg amide bond might be changed or the Cys-Arg amide proton might be required for high activity.

Olefin-Bridged Cyclic Peptides. Cyclic analogues that were bridged by an olefin instead of a disulfide in **15e** and **16e** were synthesized. C-Terminal-amidated compounds, **20a-c**, which differ in bridge length, and a C-terminal tyramide-type compound, **20d**, showed lower activity (IC_{50} = 1−10 μM), compared to those of **15e** and **16e** (Table 1). It is thought that the constraint of the olefin unit into the *E*-form is not an effective optimization component.

Analogues Constrained in the Peripheral Region of Arg^4. The significant difference of activity between **23e** ([Ala^4]-**2**, Ala-substitution for Arg^4, IC_{50} = 63 nM) and **23c** ([D-Ala^4]-**2** = [D-Ala^4]-**3**, D-Ala-substitution for L/D-Arg^4, IC_{50} = 230 nM) indicates a biological importance of the amide bond direction between D-Tyr and L/D-Arg. Thus, relationships between the conformation surrounded by Arg^4 of **2** and activity were investigated. L/D-Pro-substitutions for Arg^4 also gave the difference of activity: An L-Pro-substituted analogue, **23b**, is 4-fold stronger than a D-Pro-substituted analogue, **23a** (Table 2). N-Methylation of D-Ala^4 in **23c** (IC_{50} = 230 nM) brought about a significant increase in potency (IC_{50} of **23d** = 42 nM), which was comparable to that of **23e** ([Ala^4]-**2**) (IC_{50} = 63 nM), while N-methylation of Ala^4 in **23e** caused a significant decrease in potency (IC_{50} of **23f** = 490 nM). NMR and simulated annealing molecular dynamics (SA-MD) analysis showed that the backbone structure of **23d** is very similar to that of **23e**, but different from that of **23c**, especially in the direction of the D-Tyr-L/D-Arg amide bond (Figure 3A).[46] N-Methylation of D-Ala^4 in **23c** might cause an inversion of the D-Tyr^3-D-Ala^4 amide bond (180° rotation of ϕ and ψ torsion angles) to reduce the 1,3-pseudo-allylic strain between the side chain of D-Tyr^3 and the *N*-methyl group, resulting in a conformation that is similar to that of **23e**.

Ala-substitution for Arg^4 in **2** (**23e**) did not bring about a severe decrease in potency (IC_{50} = 63 nM),

Table 2. Inhibitory Activity of Cyclic Pentapeptides with Substitution for Arg[4] in Compound **2** against SDF-1 Binding to CXCR4

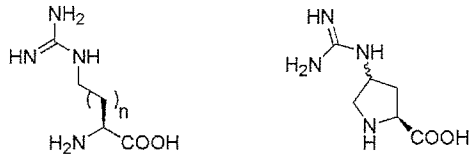

n = 1 γ-*N*-amidino-Dab (g-Dab)
n = 3 ε-*N*-amidino-Lys (g-Lys)

trans/*cis*-4-guanidino-Pro

compd	sequence[a]	$IC_{50} \pm SD$ (μM)
23a	*cyclo*(-Nal-Gly-D-Tyr-D-Pro-Arg-)	1.6 ± 0.1
23b	*cyclo*(-Nal-Gly-D-Tyr-Pro-Arg-)	0.42 ± 0.29
23c	*cyclo*(-Nal-Gly-D-Tyr-D-Ala-Arg-)	0.23 ± 0.0064
23d	*cyclo*(-Nal-Gly-D-Tyr-D-MeAla-Arg-)	0.042 ± 0.0088
23e	*cyclo*(-Nal-Gly-D-Tyr-Ala-Arg-)	0.063 ± 0.013
23f	*cyclo*(-Nal-Gly-D-Tyr-MeAla-Arg-)	0.49 ± 0.090
23g	*cyclo*(-Nal-Gly-D-Tyr-Dab-Arg-)	0.016 ± 0.010
23h	*cyclo*(-Nal-Gly-D-Tyr-Orn-Arg-)	0.019 ± 0.011
23i	*cyclo*(-Nal-Gly-D-Tyr-Lys-Arg-)	0.097 ± 0.0035
23j	*cyclo*(-Nal-Gly-D-Tyr-g-Dab-Arg-)	0.024 ± 0.0040
23k	*cyclo*(-Nal-Gly-D-Tyr-g-Lys-Arg-)	0.033 ± 0.0001
23l	*cyclo*(-Nal-Gly-D-Tyr-Asn-Arg-)	0.27
23m	*cyclo*(-Nal-Gly-D-Tyr-Gln-Arg-)	0.17
23n	*cyclo*(-Nal-Gly-D-Tyr-Glu-Arg-)	0.61
23o	*cyclo*(-Nal-Gly-D-Tyr-*trans*-4-guanidino-Pro-Arg-)	0.010 ± 0.0015
23p	*cyclo*(-Nal-Gly-D-Tyr-*cis*-4-guanidino-Pro-Arg-)	0.0099 ± 0.0043

[a] MeAla = N^{α}-Me-Ala.

whereas Ala-substitution for Nal[1], D-Tyr[3], and Arg[5] completely deminished activity of the parent compound ($IC_{50} > 1$ μM, data not shown). These results suggest that the side chain of Arg[4] in **2** has relatively little effect on the expression of activity, and that the spatial disposition of the δ-guanidino group of Arg[4] might not be optimized. Thus, several analogues, in which Arg[4] was replaced by Arg/Lys mimetics with various lengths of alkyl chains, were synthesized. Dab/L-ornithine (Orn)-substituted analogues, **23g** and **23h**, showed higher activity (IC_{50} = 16 and 19 nM, respectively) than the Ala-substituted analogue, **23e**, whereas a Lys-substituted analogue, **23i**, was slightly weaker (IC_{50} = 97 nM) than **23e** (Table 2). γ-*N*-Amidino-Dab (g-Dab)/ε-*N*-amidino-Lys (g-Lys)-substituted analogues, **23j** and **23k**, also showed higher activity (IC_{50} = 24 and 33 nM, respectively) than **23e**. However, these analogues were weaker than compound **2**, suggesting that Arg is the most suitable at position 4 among the Arg/Lys mimetics used in this study. Asn/Gln/Glu-substituted analogues, **23l**–**n**, showed a remarkable decrease in activity (IC_{50} = 270, 170, and 610 nM, respectively). This proved that a basic functional group, such as an amino or guanidino group, is necessary for strong activity in the side chain of the amino acid at position 4, and that a hydrophilic (not basic) or acidic group is not preferable to a methyl group of Ala.

Conformationally constrained Arg mimetics, *trans*-4-guanidino-Pro and *cis*-4-guanidino-Pro (Table 2), were synthesized with the idea of fixing the backbone and side chain of Arg, according to the reported procedure.[44] These Arg mimetics were incorporated in compound **2** to determine the spatial disposition of guanidino group and increase in potency. **23o** ([*trans*-4-guanidino-Pro[4]]-**2**, *trans*-4-guanidino-Pro-substitution for Arg[4]) and **23p** ([*cis*-4-guanidino-Pro[4]]-**2**, *cis*-4-guanidino-Pro-substitution for Arg[4]) showed high CXCR4-antagonistic activities (IC_{50} = 10 and 9.9 nM, respectively) that were twice as strong as that of **23j** ([g-Dab[4]]-**2**, g-Dab-substitution for Arg[4]), having the same length of the linear-type side chain of the amino acid at position 4 (IC_{50} = 24 nM), while **23b** ([Pro[4]]-**2**, Pro-substitution for Arg[4]) did not show high activity (IC_{50} = 420 nM). In consideration of the fact that the introduction of a pyrrolidinyl ring caused a significant reduction of potency (**23a** and **23b**), it is thought that fixing the side chain effectively increased potency. From these results, we have learned that the constrained guanido group might efficiently interact with CXCR4. In addition, NMR and SA-MD analysis of **23o** and **23p** showed similar dispositions of guanidino groups of *trans*/*cis*-4-guanidino-Pro residues in space (Figure 3B),[46] which might be the reason for essentially no difference in potency between **23o** and **23p**.

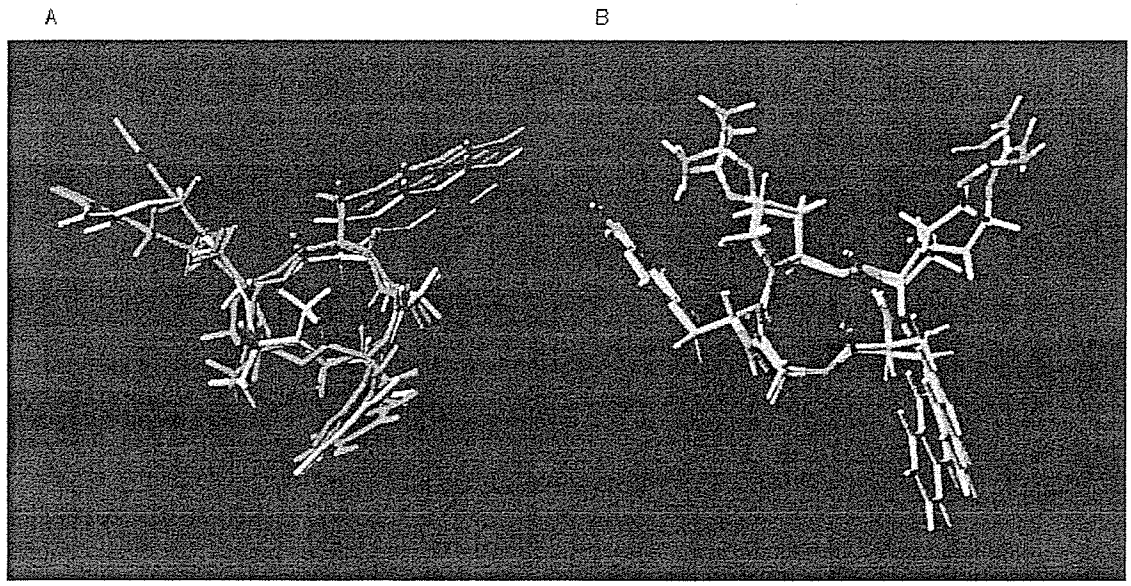

Figure 3. Superimpositions of low-energy structures of **23c** (red), **23d** (green), and **23e** (blue) (A), and **23o** and **23p** (B).

Conclusion

The fine-tuning of the ring structure of compound **2** led to findings of CXCR4 antagonists involving scaffold structures that are different from cyclic pentapeptide structures: A cyclic tetrapeptide including a γ-amino acid and pseudopeptides cyclized by disulfide and olefin bridges, having a smaller number of peptide bonds compared to compound **2**, might be useful lead compounds. Furthermore, we have learned from L/D-N^{α}-Me-Ala- and L/D-Pro-substitutions for Arg^4 that the direction of the carbonyl group in the D-Tyr^3-L/D-Ala^4 amide bonds causes a remarkable effect on CXCR4-antagonistic activity. It is also clear from this study that a basic functional group, such as amino or guanidino group, in the amino acid side-chain at position 4 is indispensable for strong activity. In addition, analogues of compound **2**, where a conformationally constrained Arg mimetic, trans- or *cis*-4-guanidino-Pro, was incorporated at position 4, showed high CXCR4-antagonistic activity, indicating that spatial constraint of a guanido group is important for an efficient interaction with CXCR4. These results for modifications of compound **2** provide useful insights for the future design of new low molecular weight CXCR4 antagonists, considering in connection with other CXCR4 antagonists. [47-53]

Experimental Section

General. ^{1}H NMR spectra were recorded using a JEOL EX-270, a JEOL AL-400, or a JNM-ECA600 spectrometer at 270, 400, or 600 MHz ^{1}H frequency, respectively, in $CDCl_3$ or DMSO-d_6. Chemical shifts are reported in parts per million downfield from internal tetramethylsilane. Nominal (LRMS) and exact mass (HRMS) spectra were recorded on a JEOL JMS-01SG-2 or JMS-HX/HX 110A mass spectrometer. Ionspray (IS)-mass spectrum was obtained with a Sciex API*III*E triple quadrupole mass spectrometer (Toronto, Canada). Optical rotations were measured in $CHCl_3$ or H_2O with a JASCO DIP-360 digital polarimeter (Tokyo, Japan) or a Horiba high-sensitive polarimeter SEPA-200 (Kyoto, Japan). For flash column chromatography, silica gel 60 H (silica gel for thin-layer chromatography, Merck) and Wakogel C-200 (silica gel for column chromatography, Wako Pure Chemical Industries, Ltd., Osaka, Japan) were employed. HPLC solvents were H_2O and CH_3CN, both containing 0.1% (v/v) TFA. For analytical HPLC, a Cosmosil 5C18-AR column (4.6 × 250 mm, Nacalai Tesque Inc., Kyoto, Japan) was eluted with a linear gradient of CH_3CN at a flow rate of 1 mL/min on a Waters model 600 (Nihon Millipore, Ltd., Tokyo, Japan). Preparative HPLC was performed on a Waters Delta Prep 4000 equipped with a Cosmosil 5C18-AR column (20 × 250 mm, Nacalai Tesque Inc.) using an isocratic mode of CH_3CN at a flow rate of 15 mL/min.

[1-(*N*,*N*-Methoxy-methyl-carbamoyl)-2(*S*)-(2-naphthyl)-ethyl]-carbamic Acid *tert*-Butyl Ester (Boc-Nal-NMe (OMe)) (4). To a stirred solution of L-3-(2-naphthyl)alanine (10.0 g, 46.4 mmol) in THF–H_2O (1:1 (v/v), 200 mL) were added triethylamine (12.5 mL, 92.9 mmol) and Boc_2O (9.63 g, 44.1 mmol) at room temperature, and the mixture was stirred at this temperature overnight. The reaction mixture was concentrated under reduced pressure. The residue was extracted with EtOAc, and the extract was washed successively with saturated aqueous citric acid, aq. 5% citric acid (× 3), H_2O (× 5), and brine and dried over $MgSO_4$. Concentration under reduced pressure gave the crude product as a white powder, which was used directly in the following step without purification. To a solution of the crude product in DMF (150 mL) were added *N*,*O*-dimethylhydroxylamine hydrochloride (10.3 g, 106 mmol), triethylamine (14.3 mL, 106 mmol), HOBt (8.11 g, 52.9 mmol), and DCC (11.8 g, 53.0 mmol) at 0 °C, and the mixture was stirred at room temperature overnight. The reaction mixture was filtered, and the filtrate was concentrated under reduced pressure. The residue was extracted with EtOAc, and the extract was washed successively with saturated aqueous citric acid, brine, saturated aqueous $NaHCO_3$, and brine and dried over $MgSO_4$. Concentration under reduced pressure followed by flash chromatography over silica gel with EtOAc–*n*-hexane (2:3) and subsequent recrystalization with Et_2O–*n*-hexane gave 12.8 g (35.7 mmol, 77% yield from L-3-(2-naphthyl)alanine) of **4** as colorless crystals. mp: 110–111 °C; $[\alpha]^{35}_D$ +29.41 (*c* 0.714, $CHCl_3$); ^{1}H NMR (400 MHz, $CDCl_3$) δ 7.73-7.82 (m, 3H), 7.62, (s, 1H), 7.39–7.48 (m, 2H), 7.31 (dd, J = 8.6, 1.5 Hz, 1H), 5.17–5.24 (br d, 1H), 5.06 (br, 1H), 3.66 (s, 3H), 3.01–3.25 (m, 4H), 1.36 (s, 9H); Anal. Calcd for $C_{20}H_{26}N_2O_6$: C, 67.02; H, 7.31; N, 7.82. Found: C, 66.78; H, 7.47; N, 7.68.

(2*E*,4*S*)-*N*-Boc-4-amino-5-(2-naphthyl)-2-pentenoic Acid *tert*-Butyl Ester (5). To a stirred solution of **4** (7.00 g, 19.5 mmol) in CH_2Cl_2 (50 mL) was added dropwise a solution of DIBAL-H in toluene (1.0 M, 38.6 mL, 38.6 mmol) at −78 °C under argon, and the mixture was stirred at −78 °C for 2 h. The reaction was quenched with saturated aqueous citric acid (50 mL) at −78 °C, and the organic solvents were concentrated under reduced pressure. The residue was extracted with EtOAc, and the extract was washed successively with brine, aq. 50% $NaHCO_3$, and brine and dried over $MgSO_4$. Concentration under reduced pressure gave the crude aldehyde as a white solid, which was used directly in the following step without purification. To a stirred suspension of LiCl (1.65 g, 39.0 mmol) in CH_3CN (30 mL) were added $(EtO)_2P(O)CH_2CO_2Bu^t$ (6.31 mL, 39.0 mmol) and DIPEA (6.79 mL, 39.0 mmol) at 0 °C under argon, and the mixture was stirred at 0 °C for 1 h. The above aldehyde in CH_3CN (30 mL) was added to the mixture at 0 °C, and the mixture was allowed to warm to room temperature and stirred overnight. The reaction mixture was concentrated under reduced pressure. The residue was extracted with EtOAc, and the extract was washed successively with saturated aqueous citric acid, brine, saturated aqueous $NaHCO_3$, and brine and dried over $MgSO_4$. Concentration under reduced pressure followed by flash chromatography over silica gel with EtOAc–*n*-hexane (1:4) and subsequent recrystalization with Et_2O–*n*-hexane gave 6.05 g (15.2 mmol, 78% from **4**) of **5** as colorless crystals. mp: 135–137 °C; $[\alpha]^{35}_D$ −12.84 (*c* 0.467, $CHCl_3$); ^{1}H NMR (400 MHz, $CDCl_3$) δ 7.72–7.87 (m 3H), 7.62 (s, 1H), 7.39–7.51 (m, 2H), 7.31 (dd, J = 8.6, 1.7 Hz, 1H), 6.85 (dd, J = 15.6, 5.1 Hz, 1H), 5.81 (dd, J = 15.6, 1.5 Hz, 1H), 4.69 (br, 1H), 4.57 (br, 1H), 2.94–3.12 (m, 2H), 1.46 (s, 9H), 1.36 (s, 9H); Anal. Calcd for $C_{24}H_{31}NO_4$: C, 72.58; H, 7.86; N, 3.52. Found: C, 72.44; H, 7.86; N, 3.22.

(2*E*,4*S*)-*N*-Fmoc-4-amino-5-(2-naphthyl)-2-pentenoic Acid (6). 5 (1.00 g, 2.51 mmol) was treated with aq. 95% TFA (20 mL) at room temperature for 2.5 h. TFA was removed under reduced pressure, and the residue was dissolved in DMF–H_2O–CH_3CN (9:1:15 (v/v), 24 mL). To the stirred solution were added DIPEA (876 μL, 5.03 mmol) and Fmoc-OSu (891 mg, 2.64 mmol) at 0 °C, and the reaction mixture was stirred at room temperature for 6 h. The mixture was concentrated under reduced pressure and acidified with aq. 1 M HCl. The mixture was extracted with EtOAc, and the extract was washed successively with aq. 0.1 M HCl (× 3) and brine and dried over $MgSO_4$. After removal of the solvent under reduced pressure, the resulting crude product was purified by flash chromatography on silica gel with $CHCl_3$–MeOH (20:1) and subsequent recrystalization with ($CHCl_3$–*n*-hexane–MeOH) to give 345.1 mg (0.753 mmol, 30% yield from **5**) of **6** as colorless crystals. mp: 189–190 °C; $[\alpha]^{34}_D$ −15.33 (*c* 0.326, $CHCl_3$); ^{1}H NMR (400 MHz, DMSO-d_6) δ 12.3 (br, 1H), 7.67–7.95 (m, 7H), 7.51–7.62 (m, 2H) 7.40–7.51 (m, 3H), 7.30–7.41 (m, 2H) 7.08–7.30 (m, 2H), 6.86 (dd, J = 15.6, 5.4 Hz, 1H), 5.81 (d, J = 15.6 Hz,1H), 4.43–4.61 (m, 1H), 4.04–4.26 (m, 3H), 3.00–3.14 (m, 1H), 2.83–3.00 (m, 1H); LRMS (FAB), *m/z* 464 (MH^+, base peak), 307, 179, 165, 154, 136, 141, 136, 121, 107, 91, 89, 77; HRMS (FAB), *m/z* calcd for $C_{30}H_{26}NO_4$ (MH^+): 464.1862, found: 464.1853.

***N*-Boc-4(*R*)-amino-5-(2-naphthyl)-pentanoic Acid *tert*-Butyl Ester (7).** To the solution of **5** (2.50 g, 6.29 mmol) in

EtOAc (100 mL) was added 10% Pd/C (200 mg). The reaction vessel was charged with atmosphere of H_2 (balloon), and the mixture was stirred at room temperature for 8 h. Completion of the reaction was monitored by RP-HPLC. The reaction mixture was filtered through a pad of Celite, rinsing with EtOAc, and the filtrate was concentrated under reduced pressure. The resulting crude product was purified by flash chromatography on silica gel with EtOAc–*n*-hexane (1:5) and subsequent recrystalization with Et_2O–*n*-hexane to give 1.87 g (4.65 mmol, 74%) of **7** as colorless crystals. mp: 90–91 °C; $[\alpha]^{35}_D$ −20.83 (*c* 0.432, $CHCl_3$); ^1H NMR (400 MHz, $CDCl_3$) δ 7.71–7.86 (m, 3H), 7.62 (s, 1H), 7.38–7.52 (m, 2H), 7.34 (d, J = 8.1 Hz, 2H), 4.42–4.58 (br d, 1H), 2.94–3.09 (m, 1H), 2.79–2.94 (m, 1H), 2.28 (t, 2H), 1.56–1.92 (m, 2H), 1.41 (s, 9H), 1.39 (s, 9H); Anal. Calcd for $C_{24}H_{33}NO_4$: C, 72.15; H, 8.33; N, 3.51. Found: C, 71.92; H, 8.49; N, 3.21.

***N*-Fmoc-4(*R*)-amino-5-(2-naphthyl)-pentanoic Acid (8).** **7** (1.00 g, 2.50 mmol) was treated with aq. 95% TFA (20 mL) at room temperature for 2.5 h. TFA was removed under reduced pressure, and the residue was dissolved in DMF–H_2O–THF (9:1:10 (v/v), 20 mL). To the stirred solution were added DIPEA (1.03 mL, 5.89 mmol) and Fmoc-OSu (1.29 g, 3.83 mmol) at 0 °C, and the reaction mixture was stirred at room temperature overnight. The mixture was concentrated under reduced pressure and acidified with aq. 1 M HCl. The mixture was extracted with EtOAc, and the extract was washed successively with aq. 0.1 M HCl (× 3) and brine and dried over $MgSO_4$. After removal of the solvent under reduced pressure, the resulting crude product was purified by flash chromatography on silica gel with $CHCl_3$–MeOH (20:1) and subsequent recrystalization with ($CHCl_3$–*n*-hexane) to give 747.6 mg (1.60 mmol, 64% yield from **7**) of **8** as colorless crystals. mp: 167–169 °C; $[\alpha]^{34}_D$ −7.31 (*c* 0.410, $CHCl_3$); ^1H NMR (400 MHz, DMSO-d_6) δ 7.73–7.92 (m 5H), 7.67 (s, 1H), 7.56–7.62 (m, 2H) 7.41–7.48 (m, 2H), 7.33–7.41 (m, 3H), 7.18–7.33 (m, 3H), 4.06–4.24 (m, 3H), 3.76 (br, 1H), 2.85 (d, J = 6.6 Hz, 2H), 2.14–2.32 (m, 2H), 1.68–1.82 (m, 1H), 1.54–1.68 (m, 1H); LRMS (FAB), *m/z* 466 (MH^+, base peak), 179, 154, 136, 141, 136; HRMS (FAB), *m/z* calcd for $C_{30}H_{28}NO_4$ (MH^+): 466.2018, found: 464.2024.

Representative Procedure for the Synthesis of γ-Amino Acid-Containing Cyclic Tetrapeptides (11a). Cl-Trt-(2-Cl) resin (1.25 mmol/g, 400 mg, 0.5 mmol) was treated with Fmoc-γ-Nal-OH (256 mg, 0.55 mmol) and DIPEA (383 μL, 2.2 mmol) in CH_2Cl_2 (4 mL) at room temperature for 2 h to yield Fmoc-γ-Nal-Trt(2-Cl) resin (0.79 mmol/g, 97%). Protected peptide **11a** resin was manually constructed by Fmoc-based solid-phase peptide synthesis on Fmoc-γ-Nal-Trt(2-Cl) resin (0.79 mmol/g, 127 mg, 0.1 mmol). Bu^t for Tyr and Pbf for Arg were employed for side-chain protection. The protected peptide **11a** resin was treated with 1,1,1,3,3,3-hexafluoro-2-propanol (HFIP)–DCM (1:4 (v/v), 7 mL) at room temperature for 2 h. After filtration, the filtrate was concentrated under reduced pressure to give the crude protected linear peptide. To a stirred mixture of the protected peptide and *N*-methylmorphorine (54.9 μL, 0.5 mmol) in DMF (25 mL) was added diphenylphosphoryl azide (DPPA) (53.2 μL, 0.247 mmol) at −40 °C. The reaction mixture was stirred for 24 h with warming up to room temperature and concentrated under reduced pressure. The residue was subjected to solid-phase extraction over basic alumina in $CHCl_3$–MeOH (9:1) to remove inorganic salts derived from DPPA. The resulting cyclic protected peptide was treated with aq. 95% TFA (10 mL) at room temperature for 2 h. Concentration under reduced pressure and purification by HPLC gave the cyclic pseudopeptide **11a** (42.9 mg, 61% yield from Fmoc-γ-Nal-Trt(2-Cl) resin) as a freeze-dried powder.

Fmoc-tyramine-Wang PEG Resin. To a mixture of Wang PEG resin (0.33 mmol/g, 1.82 g, 0.600 mmol), Fmoc-tyramine (647 mg, 1.80 mmol), Ph_3P (472 mg, 1.80 mmol), and *N*-methylmorphorine (66.0 μL, 0.600 mmol) in CH_2Cl_2–THF (3:1 (v/v), 16 mL) was added diisopropyl azodicarboxylate (DIAD) (40% solution in toluene, 886 μL, 1.80 mmol) at 0 °C. The reaction mixture was stirred at room temperature for 2 d. The obtained resin was washed with THF (20 mL × 3), DMF (20 mL × 3), MeOH (20 mL × 3), $CHCl_3$ (20 mL × 3) and Et_2O (20 mL × 3) and dried in vacuo. The loading rate of the resin was estimated by Fmoc-quantification (0.126 mmol/g (41%)).

Representative Procedure for the Synthesis of Disulfide-Bridged Cyclic Peptides (16e). Protected peptide resin was manually constructed by Fmoc-based solid-phase peptide synthesis on Fmoc-tyramine-Wang PEG resin (0.126 mmol/g, 397 mg, 0.05 mmol). Fmoc-β-Ala-OH was condensed to the N-terminal amino group of H-Cys-Arg(Pbf)-Nal-D-Cys-tyramine-Wang PEG resin, and Fmoc group was deprotected by treatment with 20% piperidine in DMF (20 min). To a mixture of the resin and DIPEA (52,5 μL, 0.300 mmol) in DMF (5 mL) was added 1*H*-pyrazole-1-carboxamidine hydrohloride (22.0 mg, 0.150 mmol) at room temperature. The reaction mixture was stirred at room temperature for 12 h. This N-guanylation procedure was repeated once again. The protected resin was treated with EDT/H_2O/TFA (2.5:2.5:95 (v/v), 6 mL) at 0 °C for 2 h. The reaction mixture was filtered, and the filtrate was concentrated by bubbling with N_2 gas. Cooled Et_2O was added to the residue, and the resulting precipitate was separated by centrifugation. The precipitate was washed with Et_2O three times. The crude peptide was dissolved in H_2O, and pH of this solution was adjusted to approximately 8 with aq. 0.28% NH_3. Air oxidation for 1 d and purification by HPLC gave the cyclic pseudopeptide **16e** (6.5 mg, 16% yield from Fmoc-tyramine-Wang PEG resin) as a freeze-dried powder.

Synthesis of 15q. Protected peptide resin was manually constructed by Fmoc-based solid-phase peptide synthesis on Fmoc-HN-Rink amide resin (0.36 mmol/g, 139 mg, 0.05 mmol). To a suspension of H-Cys-Arg(Pbf)-Nal-D-Cys-HN-Rink amide resinin DCM were added *N*-Fmoc-3-aminopropanal (44.0 mg, 0.15 mmol) and $NaBH(OAc)_3$ (53.0 mg, 0.25 mmol) at room temperature. The mixture was stirred at room-temperature overnight. Deprotection of the Fmoc group, N-guanylation, deprotection/cleavage from the resin, air oxidation, and HPLC purification were performed by use of a procedure identical with that described for the synthesis of **16e** to yield the cyclic pseudopeptide **15q** (3.0 mg, 9% yield from Fmoc-HN-Rink amide resin) as a freeze-dried powder.

Representative Procedure for the Synthesis of Olefin-Bridged Cyclic Peptides (20a). Protected peptide resin was manually constructed by Fmoc-based solid-phase peptide synthesis on Fmoc-HN-Rink amide resin (0.29 mmol/g, 172 mg, 0.05 mmol). Fmoc-β-Ala-OH was condensed to the N-terminal amino group of H-L-2-allylGly-Arg(Pbf)-Nal-D-2-allylGly-HN-Rink amide resin. To a suspension of the protected resin in dry DCM (5 mL) was added Grubbs catalyst second generation (4.20 mg, 5.00 μmol) at room temperature under argon. The reaction mixture was refluxed for 9 h. After removal of the organic solvent, this reaction was repeated once again for 12 h in the presence of the catalyst (21 mg, 0.025 mmol) in dry DCM (5 mL). The obtained resin was treated with 20% piperidine in DMF (20 min). To a mixture of the resin and DIPEA (52.5 μL, 0.300 mmol) in DMF was added 1*H*-pyrazole-1-carboxamidine hydrohloride (22.0 mg, 0.15 mmol) at room tempereture. The reaction mixture was stirred at room temperature for 12 h. This N-guanylation procedure was repeated once again. The protected resin was treated with thioanisole (940 μL), TFA (7.2 mL), and TMSBr (1.32 mL) at 0 °C for 2 h. The reaction mixture was filtered, and the filtrate was concentrated by bubbling with N_2 gas. Cooled Et_2O was added to the residue, and the resulting precipitate was separated by centrifugation. The precipitate was washed with Et_2O. The crude peptide was purified by HPLC to give the cyclic pseudopeptide **20a** (3.3 mg, 10% yield from Fmoc-HN-Rink amide resin) as a freeze-dried powder.

Representative Procedure for the Synthesis of Cyclic Pentapeptides (*cyclo*(-D-Tyr-Pro-Arg-Nal-Gly-) (23b)). Protected peptide resin was manually constructed by Fmoc-based solid-phase peptide synthesis on Fmoc-Gly-Trt(2-Cl) resin (0.741 mmol/g, 101 mg, 0.075 mmol). Bu^t for Tyr and Pbf for Arg were employed for side-chain protection. Cleavage from the resin, cyclization, deprotection, and HPLC purification were performed by use of a procedure identical with that

described for the synthesis of **11a** to yield the cyclic peptide **23b** (25.2 mg, 50% yield from Fmoc-Gly-Trt(2-Cl) resin) as a freeze-dried powder.

Representative Procedure for the Synthesis of *N*-Methylated Cyclic Pentapeptides (*cyclo*(-D-Tyr-D-MeAla-Arg-Nal-Gly-) (23d)). According to a procedure identical with that described for the preparation of **23b**, **23d** was synthesized except for N-methylation of the D-Ala residue. N-Methylation was performed by the Fukuyama–Mitsunobu reaction:[28] To a mixture of H-D-Ala-Arg(Pbf)-Nal-Gly-Trt(2-Cl) resin (0.075 mmol) and *o*-nitrobenzenesulfonyl chloride (49.9 mg, 0.225 mmol) in CH_2Cl_2 (5 mL) was added 2,4,6-collidine (49.6 μL, 0.375 mmol) at room temperature. The reaction mixture was stirred at room temperature for 2 h, and the resin was washed successively with CH_2Cl_2 (10 mL × 3) and DMF (10 mL × 3). To a mixture of the resin, Ph_3P (98.4 mg, 0.375 mmol), and MeOH (15.2 μL, 0.375 mmol) in dry THF (5 mL) was added diethyl azodicarboxylate (DEAD) (40% solution in toluene, 170 μL, 0.375 mmol) at 0 °C. The reaction mixture was stirred at room temperature for 2 h. The resin was washed successively with THF (10 mL × 3) and DMF (10 mL × 3). To a mixture of the resin and DBU (56.1 μL, 0.375 mmol) in DMF (5 mL) was added 2-mercaptoethanol (51.4 μL, 0.750 mmol) at room temperature, and the reaction mixture was stirred at room temperature for 2 h. Subsequent condensation of the next residue (D-Tyr) to the secondary amino group on the resin was performed by treatment with Fmoc-D-Tyr(Bu^t)-OH (5 equiv), HATU (4.9 equiv), HOAt (5 equiv), and DIPEA (10 equiv) in DMF (5 mL) for 1 h (× 2). **23d** (freeze-dried powder): 3.0 mg, 6.0% yield from Fmoc-Gly-Trt(2-Cl) resin.

(2S,4S)-N^{α}-Cbz-4-*N*-Boc-aminoproline Benzyl Ester. (2*S*,4*S*)-N^{α}-Cbz-4-aminoproline benzyl ester (1.44 g, 3.93 mmol), which was prepared from (2*S*,4*S*)-N^{α}-Cbz-4-azidoproline benzyl ester according to Tamaki's procedure,[35] was dissolved in THF (20 mL), and Boc_2O (1.38 g, 6.31 mmol) and triethylamine (1.10 mL, 7.89 mmol) were added to the solution at 0 °C. The reaction mixture was stirred at room temperature for 7.5 h. The mixture was concentrated under reduced pressure, and the residue was extracted with Et_2O. The extract was washed successively with saturated aqueous citric acid (× 2), H_2O (× 2), and brine and dried over $MgSO_4$. After removal of the solvent under reduced pressure, the resulting crude product was purified by flash chromatography on silica gel with EtOAc–*n*-hexane (1:4) to give 1.70 g (3.77 mmol, 96% yield) of the title compound as a colorless oil. $[\alpha]^{29}_D$ −39.47 (*c* 0.304, $CHCl_3$); ^{1}H NMR (400 MHz, $CDCl_3$) δ 7.18–7.45 (m, 10H), 4.95–5.40 (m, 5H), 4.28–4.50 (m, 2H), 3.68–3.82 (m, 1H), 3.44–3.60 (m, 1H), 2.39–2.57 (m, 1H), 1.89–2.05 (m, 1H), 1.45 (s, 9H); LRMS (FAB), *m/z* 477 (MNa^+, base peak), 455 (MH^+), 445, 399, 355, 91; HRMS (FAB), *m/z* calcd for $C_{25}H_{31}N_2O_6$ (MH^+): 455.2182, found: 455.2186.

(2S,4S)-N^{α}-Fmoc-4-*N*-Boc-aminoproline. (2*S*,4*S*)-N^{α}-Cbz-4-*N*-Boc-aminoproline benzyl ester (1.70 g, 3.77 mmol) was dissolved in EtOH (80 mL), and 5% Pd/C (170 mg) was added to the solution. The reaction vessel was charged with atmosphere of H_2 (balloon), and the mixture was stirred at room temperature for 12 h. After removal of Pd/C by filtration, the filtrate was concentrated under reduced pressure to give the crude product as a colorless oil, which was used directly in the following step without purification. To the crude product in H_2O–THF (4:3 (v/v), 70 mL) were added triethylamine (1.41 mL, 7.55 mmol) and Fmoc-OSu (2.54 g, 7.55 mmol) in CH_3CN (10 mL) at 0 °C, and the reaction mixture was stirred at room temperature for 2 h. The mixture was acidified with saturated aqueous citric acid and concentrated under reduced pressure. The residue was extracted with EtOAc, and the extract was washed successively with saturated aqueous citric acid, H_2O (× 3), and brine and dried over $MgSO_4$. After removal of the solvent under reduced pressure, the resulting crude product was purified by flash chromatography on silica gel with $CHCl_3$–MeOH (20:1) to give 1.18 g (2.60 mmol, 69% yield) of the title compound as colorless crystals. mp: 87–89 °C; $[\alpha]^{24}_D$ −33.81 (*c* 0.621, $CHCl_3$); ^{1}H NMR (400 MHz, DMSO-d_6) δ 8.30 (s, 1H), 7.82–7.97 (m, 2H), 7.57–7.75 (m, 2H), 7.25–7.49 (m, 4H), 3.93–4.36 (m, 5H), 3.60–3.75 (m, 1H), 3.05–3.21 (m, 1H), 2.32–2.58 (m, 1H), 1.67–1.90 (m, 1H), 1.44 (s, 9H); LRMS (FAB), *m/z* 451 [$(M - H)^-$], 229, 155, 153, 152 (base peak); HRMS (FAB), *m/z* calcd for $C_{25}H_{27}N_2O_6$ [$(M - H)^-$]: 451.1868, found: 451.1883.

(2S,4*R*)-N^{α}-Cbz-4-*N*-Boc-aminoproline Benzyl Ester. By use of a procedure identical with that described for the preparation of (2*S*,4*S*)-N^{α}-Cbz-4-*N*-Boc-aminoproline benzyl ester, (2*S*,4*R*)-N^{α}-Cbz-4-aminoproline benzyl ester (5.56 g, 15.7 mmol) was converted into 6.24 g (13.8 mmol, 88% yield) of the title compound as colorless crystals. mp: 97–99 °C; $[\alpha]^{25}_D$ −47.61 (*c*, 0.714, $CHCl_3$); ^{1}H NMR (400 MHz, $CDCl_3$) δ 7.15–7.43 (m, 10H), 4.93–5.27 (m, 4H), 4.56–4.70 (br, 1H), 4.37–4.54 (m, 1H), 4.21–4.35 (br, 1H), 3.78–3.89 (m, 1H), 3.30–3.50 (m, 1H), 2.12–2.34 (m, 2H), 1.45 (s, 9H); LRMS (FAB), *m/z* 477 (MNa^+, base peak), 455 (MH^+), 445, 399, 355, 263, 91; HRMS (FAB), *m/z* calcd for $C_{25}H_{31}N_2O_6$ (MH^+): 455.2182, found: 455.2176.

(2S,4*R*)-N^{α}-Fmoc-4-*N*-Boc-aminoproline. By use of a procedure identical with that described for the preparation of (2*S*,4*S*)-N^{α}-Fmoc-4-*N*-Boc-aminoproline, (2*S*,4*R*)-N^{α}-Cbz-4-*N*-Boc-aminoproline benzyl ester (2.75 g, 6.10 mmol) was converted into 2.05 g (4.51 mmol, 74% yield) of the title compound as colorless crystals. mp: 85–87 °C; $[\alpha]^{24}_D$ −36.92 (*c* 0.325, $CHCl_3$); ^{1}H NMR (400 MHz, $CDCl_3$) δ 8.33 (s, 1H), 7.82–7.97 (m, 2H), 7.56–7.72 (m, 2H), 7.26–7.49 (m, 4H), 3.96–4.36 (m, 4H), 3.50–3.67 (m, 1H), 3.18–3.40 (m, 2H), 1.99–2.26 (m, 2H), 1.44 (s, 9H); LRMS (FAB), *m/z* 451 [$(M - H)^-$], 229, 155, 153, 151 (base peak); HRMS (FAB), *m/z* calcd for $C_{25}H_{27}N_2O_6$ [$(M - H)^-$]: 451.1868, found: 451.1887.

Representative Procedure for the Synthesis of Cyclic Pentapeptides Containing Arginine Mimetic (*cyclo*(-D-Tyr-*trans*-4-guanidino-Pro-Arg-Nal-Gly-) (23o)). According to a procedure identical with that described for the preparation of **23b**, the cyclic protected peptide was synthesized. The obtained protected peptide (0.05 mmol) was treated with aq. 95% TFA (5 mL) for 2 h at room temperature, and concentration under reduced pressure gave the crude cyclic peptide. To a mixture of the crude product and 1*H*-pyrazole-1-carboxamidine hydrochloride (22.0 mg, 0.15 mmol) in DMF (4 mL) was added DIPEA (52.3 μL, 0.300 mmol) at room temperature. The reaction mixture was stirred at room temperature for 12 h. This procedure (N-guanylation of the γ-amino group of the *trans*-4-amino-Pro residue) was repeated once again. Concentration under reduced pressure and purification by HPLC gave the cyclic peptide **23o** (5.1 mg, 14% yield from Fmoc-Gly-Trt(2-Cl) resin) as a freeze-dried powder.

[^{125}I]-SDF-1 Binding and Displacement. Stable CHO cell transfectants expressing CXCR4 variants were prepared as described previously.[54] CHO transfectants were harvested by treatment with trypsin-EDTA, allowed to recover in complete growth medium (MEM-α, 100 μg/mL penicillin, 100 μg/mL streptomycin, 0.25 μg/mL amphotericin B, 10% (v/v)) for four to 5 h and then washed in cold binding buffer (PBS containing 2 mg/mL BSA). For ligand binding, the cells were resuspended in binding buffer at 1×10^7 cells/mL, and 100 μL aliquots were incubated with 0.1 nM of [^{125}I]-SDF-1 (PerkinElmer Life Sciences) for 2 h on ice under constant agitation. Free and bound radioactivity were separated by centrifugation of the cells through an oil cushion and bound radioactivity was measured with a gamma-counter (Cobra, Packard, Downers Grove, IL). Inhibitory activity of test compounds was determined based on the inhibition of [^{125}I]-SDF-1-binding to CXCR4 transfectants (IC_{50}).

NMR Spectroscopy (23c–e, 23o, and 23p). The peptide sample was dissolved in DMSO-d_6 at a concentration of 5 mM. ^{1}H NMR spectra of the peptides were recorded at 300 K. The assignments of the proton resonances were achieved by use of ^{1}H–^{1}H COSY spectra. $^3J(H^N,H^{\alpha})$ coupling constants were measured from one-dimensional spectra. The mixing time for the NOESY experiments was set at 400 ms. NOESY spectra were composed of 512 real points in the F2 dimension and 256 real points, which were zero-filled to 256 points in the F1 dimension, with 144 scans per t1 increment. The cross-peak